Alexander Novikov

Testing and evaluation of distance protection in system with high PV sources penetration

Master of Science Thesis

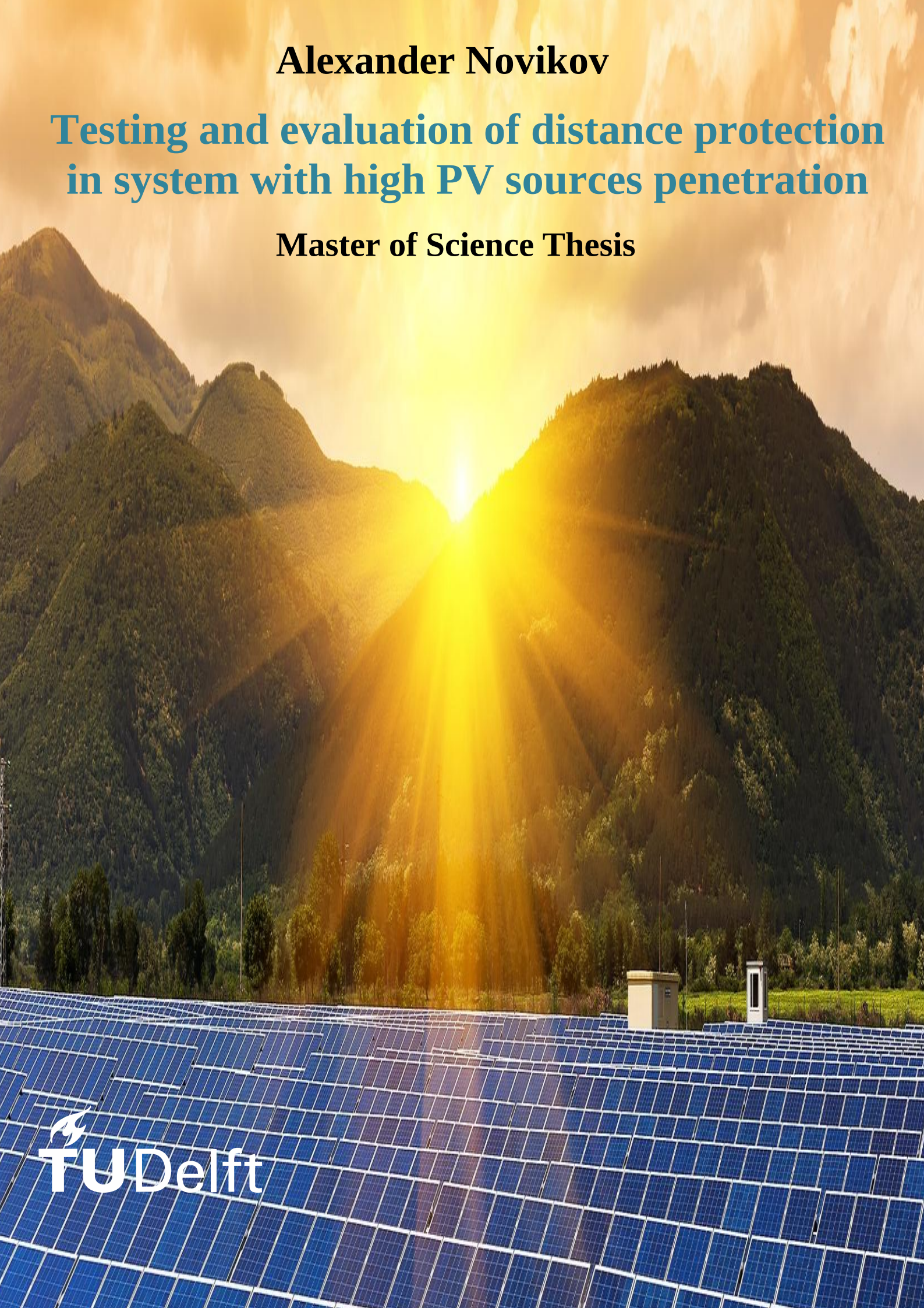

TU Delft

Testing and evaluation of distance protection in system with high PV sources penetration

By

Alexander Novikov

in partial fulfilment of the requirements for the degree of

Master of Science

in Electrical Engineering

at the Delft University of Technology

Intelligent Electrical Power Grids (IEPG) Research Group

Department of Electrical Sustainable Energy (ESE)

Faculty of Electrical Engineering, Mathematics, and Computer Science (EEMCS)

To be defended publicly on Monday July 9, 2018 at 10:00 AM.

Supervisor:	Prof. Dr. Ir. Marjan Popov	
Thesis committee:	Prof. Dr. Ir. Marjan Popov,	TU Delft
	Prof. Dr. Ir. Jose Rueda Torres,	TU Delft
	Prof. Dr. Armando Rodrigo Mor,	TU Delft
	Dr. Ir. Jose Chavez Muro,	TU Delft

Contents

List of Figures

List of Tables

Abstract

This thesis investigates the performance of distance protection function of actual relay placed on high voltage 400 kV transmission line in a system with high photovoltaic (PV) sources penetration.

The benchmark model of system with radial connection of PV plant and conventional power plant was designed in the platform of RSCAD software.

By hardware-in-the-loop (HiL) test setup two commercial relays were connected to the Real-Time Digital Simulator (RTDS) and linked to two virtual breakers in transmission line ends modelled in RSCAD. Special logic for correct signal processing of analogical inputs and binary outputs of relays was designed and employed in RSCAD.

Several test scenarios were recreated and analysed. Distance protection function was tested with radial connection of synchronous generator to check response of benchmark system and validate correct settings of the relays. Afterwards synchronous generator was substituted by generic PV farm model. Impact of different fault locations, types of fault, power generation level and fault impedance values were studied on a basis of the benchmark model.

The goal of this research was to determine the extreme scenarios in the power system when real relay would fail to detect the fault conditions. Failures of distance protection function operation were detected and explained from mathematical side.

On the basis of this research the author revealed the cases of relay maloperation and suggested possible ways of solution to this problem by the set of recommendations.

Keywords: RTDS, hardware-in-the-loop test, distance protection function, photovoltaic plant, VSC converter

Acknowledgements

This Master Thesis was made in partial fulfilment of the requirements for the degree of Master of Science as a part of Electrical Sustainable Energy (ESE) Program at EEMCS faculty in Delft University of Technology.

I am grateful to several people who helped me to get this Master Thesis to completion.

Firstly, I would like to express gratitude to Marjan Popov for giving me an opportunity to work on this exciting project in Intelligent Electrical Power Grids (IEPG) research group.

Secondly, I want to say thank you to Jose Chavez Muro for your daily help and guidance in all related topics during my Master Thesis.

I am grateful to Global Education scholarship from Russian Ministry of Education for providing the opportunity for me to study in TU Delft.

A special gratitude goes to my family and my friends in TU Delft. Thank you very much for your advices and support during my Master Thesis.

1. Introduction

The reliable electrical energy supply is essential part of economic progress for any modern country. Overhead lines and underground cables are used for connection and supply of consumers in areas remote from main generation. Any high voltage line contingency can create supply shortage and lead to accident damage and loss of profit for Transmission System Operator (TSO) and generation companies. In worst case scenario it can cause a black-out. That is why operation of relay protection devices placed in transmission lines must be correct and meet criteria of reliability, selectivity, speed, sensitivity and interoperability.

In contemporary world the development of electrical power systems is not possible without construction of new generation stations, substations and electrical grids. Due to recent developments in power electronics and steep decline of prices on manufacturing of power electronic devices the new large-scale photovoltaic (PV) plants and wind farms construction is rapidly increased compare to traditional power plants.

In compliance with the Paris Agreement many countries are stimulating rise of renewable energy generation. For example, according to European plan on climate change [1] 20% of the energy should be produced by renewables and the 20% increase in energy efficiency should be achieved by 2020 in European Union. By 2030 the share of renewable energy must come up to the point of at least 27%.

In the North America “Climate, Clean Energy, and Environment Partnership Action” Plan was announced as mentioned in [2]. It is claimed that the goal is to achieve 50 % of clean power generation by 2025.

In Australia, based on “Emissions Reduction Target” [3] the renewable energy target allows sustainable growth in both small and large scale renewable technologies, delivering more than 23 % of Australia’s electricity from renewable sources by 2020.

In order to achieve higher generation share of renewables the new trend in development of power systems is the construction of large scale PV and wind farms with capacity of hundreds megawatts. There are many projects of large PV plants operating already like Desert Sunlight Solar Farm, Mount Signal Solar in USA, Solarpark Meuro in Germany and Sunport Delfzijl in Netherlands, etc.

All facts mentioned above give as a clear understanding that in the nearest time most of the grids will face similar problems because of increase of PV capacity in the system. For example, the intermittent nature of power converters used for the interconnection of renewable energy sources to electrical grid can cause number of challenges for distant relay protection operation.

1.1 Literature Review

First relay with distance protection function was designed by Krämer, Chr., F&G in 1904 and was based on simultaneous detection of increase in current and voltage drop [4]. The first electronic distance protection based on transistors was used in 1959 by French EdF in the 200 kV grids [5]. In 1985 the first microprocessor technology was applied in distance protection and numerical relays appeared [6].

Lately, large scale integration of renewable energy sources to transmission grids started to impact on correct operation of numerical distance relays.

One of the reasons for distance protection maloperation is the low fault current level at various locations in the network. Short circuit current contribution of PV plant was considered in [7] and conclusion was made that negative sequence current and positive sequence active current are usually suppressed to zero by the inverter control and can be changed to improve protection operation.

PV central inverter control strategy with positive and negative sequence control was introduced by [8] and the mathematical concept of control logic was explained there in details. The disadvantage of this type of control is delay in dynamic response caused by moving average filters.

Distance protection performance in overhead lines emanating from full-scale converter-interfaces renewable energy power plants was estimated in [9]. Possible solutions for enhancement of distance relay logic were suggested in [10] and tested in PSCAD software.

Maloperation of distance protection of transmission lines connected with VSC-HVDC system modelled in RSCAD was shown in [11] and different fault-ride through strategies for voltage source converters were tested in hardware-in-the-loop test in [12].

Recently, impact of renewable sources on distance protection operation during ground fault with examples of false tripping in real grid was reported in [13].

Maloperation and missed tripping of distance protection under fault conditions happens mainly because the renewable energy generation technology is interfaced to the grid through power electronic converters. The converter controls typically limit the fault current contribution to a value close to the normal rating of the converter. As such, when the renewable power output is high during certain periods of the day or year, the existing distance protection relay settings may not be suitable to meet the expected accuracy and reliability.

1.2 Objectives of Master Thesis

The main objective of this Master Thesis is the proper testing and analysis of real relay distance protection function performance with PV source radially connected to electrical system in Real-Time-Digital-Simulator (RTDS) by hardware-in-the-loop-test. Most of previous researches mentioned in literature review were based on offline simulation software's while this way of testing can provide more precise results and allow validating of relay maloperation.

The research objectives of the Master Thesis are:

1) Testing of distance protection function in system with high PV sources integration.

2) Analysis of results according to impedance trajectory and current threshold.

3) Proposal of recommendations for improvement of distance protection performance.

1.3 Research Methodology

The research considered in this Master Thesis was conducted in several stages:

1) Modelling of the transmission grid with PV source integration in RSCAD.

2) Connection of the relay with distance protection function to RTDS.

3) Testing of relay with distance protection function in system with synchronous generators.

4) Testing of relay with distance protection function in system with high PV sources integration.

5) Analysis of testing results and proposal of recommendations for improvement of distance protection performance.

1.4 Thesis Layout

Chapter 1. Introduction

This chapter presents motivation for this research, literature review of previous studies, research objectives and methodologies of Master thesis.

Chapter 2. Distance relay protection theory

This chapter introduces the basics of distance relay protection operation including fault detection, calculation of impedance and logic of numerical relay.

Chapter 3. PV model and Grid Code

This chapter shows PV model design including maximum power point tracking, control signals and small-time step blocks and Grid Code requirements.

Chapter 4. Test system model

This chapter represents description of each element of system and explains the choice of system topology.

Chapter 5. Hardware-in-the-loop test setup

This chapter shows the software modelling, the hardware connections of hardware-in-the-loop test setup and description of scripts for processing automation.

Chapter 6. Testing of distance protection

This chapter introduces the test scenarios and compilation of the results.

Chapter 7. Conclusion and recommendations

This chapter includes a set of recommendation for improvement of relay operation and directions for further research.

2. Distance Protection Theory

2.1 Introduction

The distance protection uses signals of voltages and currents measured by current transformer (CT) and voltage transformer (VT) to calculate the fault impedance and the distance of the fault inception.

When short-circuit condition appears in the electrical system the sharp drop of the voltage level and the rapid increase of currents in lines usually takes place. Thus, the impedance value measured by distance relay is much smaller during fault than during steady state condition. This is the base concept of distance protection function operation.

Distance protection is usually implemented with several zones. The main parameters for each zone are length of line and operation time. For example in Figure 2.1 the fault in point “Fault 1” should be detected by the second zone of “Relay 1” and the first zone of “Relay 2”. If coordination of zone settings is correct fault current will be isolated by “Relay 2” as it has smaller trigger time. If fault appears in point “Fault 2” then it is switched off by the first zone of “Relay 3” correspondingly.

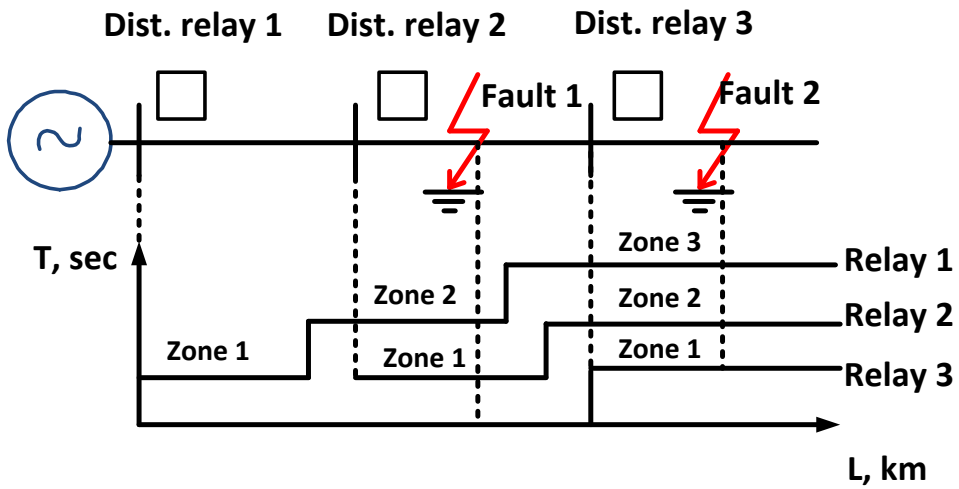

Figure 2.1 Stepped characteristic of distance protection

One century ago the relay protection engineering started with electromechanical relays to protect and isolate the parts of the grid under fault. Data processing and new materials made an evolution to new relays based on microprocessors, known as digital relays..

There are several advantages in digital relay operation. The actual solid state relays can be multifunctional devices and protect the elements of system with one or more functions. In this research the relay under consideration combine differential, distance and overcurrent protection functions in one device.

One more advantage is the possibility to exchange data between devices of different brands.

Another strong point of digital relay is the low cost of memory to store fault parameters of currents, voltages and impedance trajectories.

The digital relay is not using the continuous analogical signal for calculation. It operates with spaced in time samples of the analogical signal. The relay is designed to use different digital signal processing techniques to the observed samples. The decision for trip action is made based on calculated data from these samples.

2.2 Fault Detection

There are several concepts which can be applied for fault detection in digital relays like the data window method, the phasor method, etc. Below the concept of fault detection for relay under study is described.

The method which is employed in the commercial relay is data window method. In the data window method the moving window is used which contains three samples of data. During disturbance one prefault sample and two postfault samples are detected in the window W1 as shown in Figure 2.2.

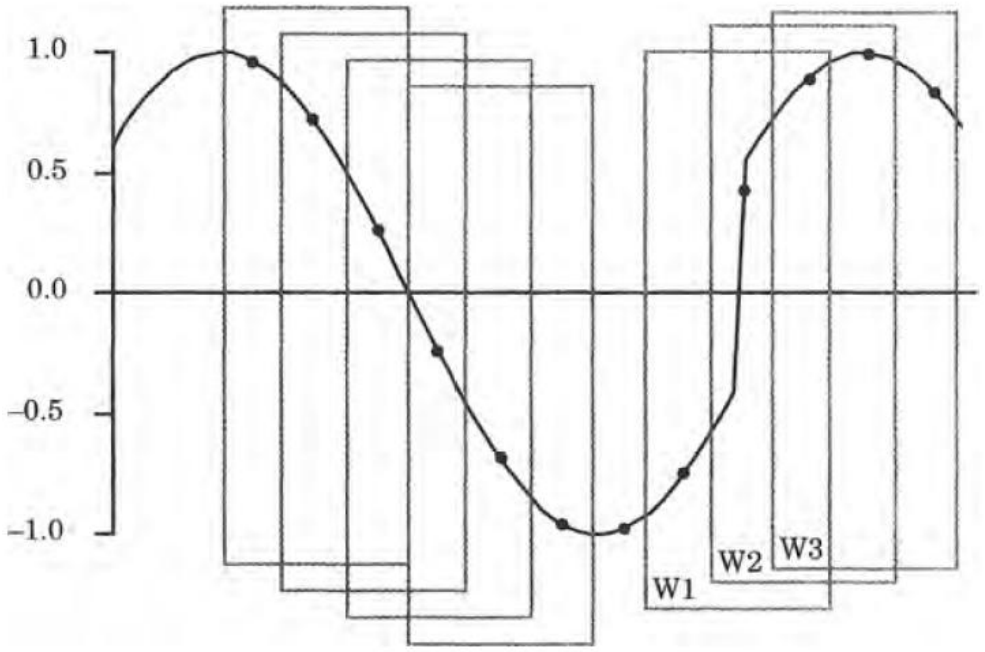

Figure 2.2 A moving three-sample window during a disturbance [6]

While all windows embracing three samples of prefault data will give the accurate phasor values, in the window W1 the wave is far from sinusoidal shape and the phasor values calculated based on this samples will have no meaning.

In relay under consideration the processor estimates window with 3 samples during the time period △t=1 ms as mentioned in [14]. Algorithms inside commercial relay are using sampling rate of 20 samples per cycle. In the system with frequency 50 Hz △t is calculated based on the equation 2.1. Sampling rate of bigger value will require higher speed processing due to complexity of computation.

$$\Delta t = \frac{1}{Sampling\ \ rate * f_{SYSTEM}} = \frac{1}{20\ \ samples * 50Hz} = 1\ \ ms \tag{2.1}$$

The other variable is the length of the data window. The window and data sequences size can influence speed of calculation. According to [6] longer windows which are giving longer sequences of sampled data require a longer time to clear the time period during which windowed sequences contain a mixture of pre and postfault data.

2.3 Impedance Calculation

The impedance calculation method in the distance protection depends on the type of fault. According to [14], a separate measuring system is used in the relay for six involved impedance loops: phase A to earth (L1-E), L2-E, L3-E, phase A to phase B (L1-L2), L2-L3, L3-L1.

Line-to-line loop impedance calculation is based on equations 2.2 and 2.3 and shown in Figure 2.3 below:

$$I_{L1} \cdot Z_L - I_{L2} \cdot Z_L = U_{L1-E} - U_{L2-E} \tag{2.2}$$

$$Z_L = \frac{U_{L1-E} - U_{L2-E}}{I_{L1} - I_{L2}} \tag{2.3}$$

where U and I are the (complex) measured quantities and $Z = R + jX$ is the line impedance.

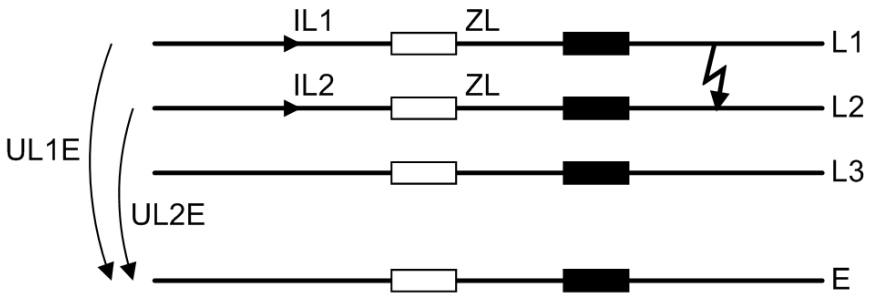

Figure 2.3 Two-lines fault clear of earth, fault loop [14]

Line-to-ground loop are calculated by equations 2.4-2.6 and shown in the Figure 2.4.

$$U_{L3-E} = I_{L3} \cdot (R_L - jX_L) - I_E \cdot (\frac{R_E}{R_L} \cdot R_L + j(\frac{X_E}{X_L}) \cdot X_L), \tag{2.4}$$

$$R_{L3-E} = \frac{U_{L3-E}}{I_{L3}} \cdot \frac{\cos(\phi_u - \phi_L) - \frac{I_E}{I_{L3}} \cdot \frac{X_E}{X_L} \cdot \cos(\phi_u - \phi_E)}{1 - (\frac{X_E}{X_L} + \frac{R_E}{R_L}) \frac{I_E}{I_{L3}} \cdot \cos(\phi_E - \phi_L) + \frac{R_E}{R_L} \cdot \frac{X_E}{X_L} \cdot (\frac{I_E}{I_{L3}})^2}, \tag{2.5}$$

$$X_{L3-E} = \frac{U_{L3-E}}{I_{L3}} \cdot \frac{\sin(\phi_u - \phi_L) - \frac{I_E}{I_{L3}} \cdot \frac{R_E}{R_L} \cdot \sin(\phi_u - \phi_E)}{1 - (\frac{X_E}{X_L} + \frac{R_E}{R_L}) \frac{I_E}{I_{L3}} \cdot \cos(\phi_E - \phi_L) + \frac{R_E}{R_L} \cdot \frac{X_E}{X_L} \cdot (\frac{I_E}{I_{L3}})^2}, \tag{2.6}$$

where

U_{L3-E} - r.m.s. value of the short-circuit voltage

I_{L3} - r.m.s. value of the phase short-circuit current

I_E - r.m.s. value of the earth short-circuit current

ϕ_u - phase angle of the short-circuit voltage

ϕ_L - phase angle of the phase short-circuit current

ϕ_E - phase angle of the earth short-circuit current

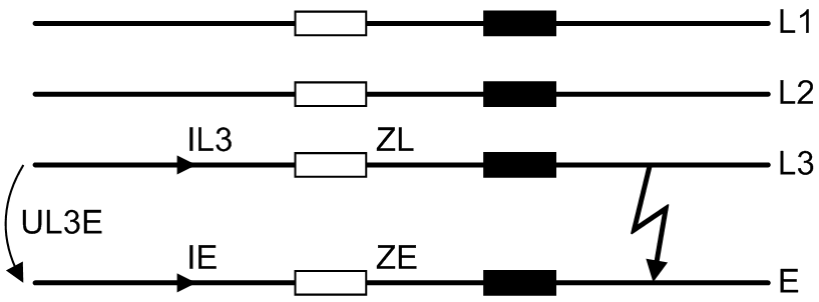

Figure 2.4 Single-phase earth fault, fault loop [14]

The factors R_E/R_L and X_E/X_L in equations 2.4-2.5 are independent from distance to fault value and consider only line parameters.

2.4 Distance Relay Operation

Distance protection is the second main function of commercial relay under consideration. Generic simplified function block of digital distance relay is shown in Figure 2.5.

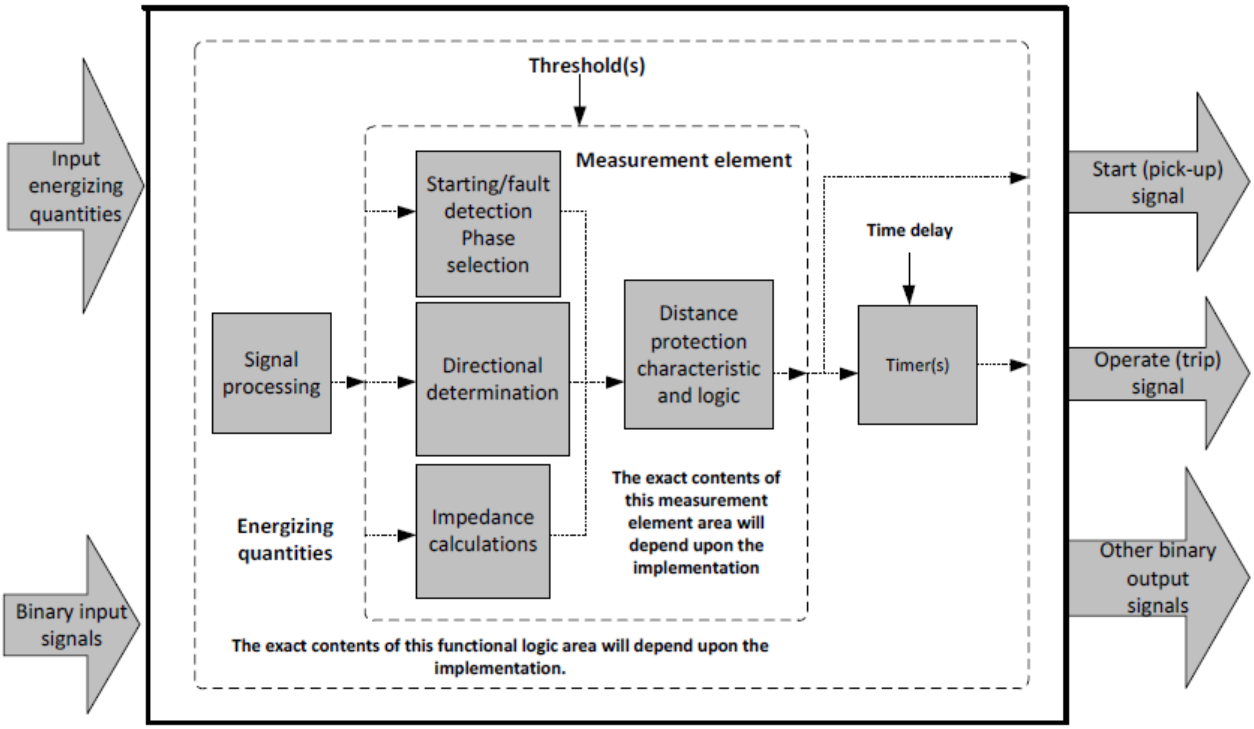

Figure 2.5 Simplified distance protection function block diagram [15]

The distance protection element operates based on the impedance calculated using the input energizing quantities: the voltage and current measurements from the grid.

The second stage is signal processing described in section 2.2 and the data window method is applied. For a distance protection relay in order to declare a fault, the following main criteria must be satisfied.

1) Current pick-up, which consist of several stages including certain duration of fault current, threshold overcurrent value and phase selection of the current which are used to enhance security

2) Directionality determination to avoid maloperation during close faults

3) Impedance reach calculated according to impedance loops mentioned in section 2.3 and speed of impedance change dz/dt when it comes to the zone.

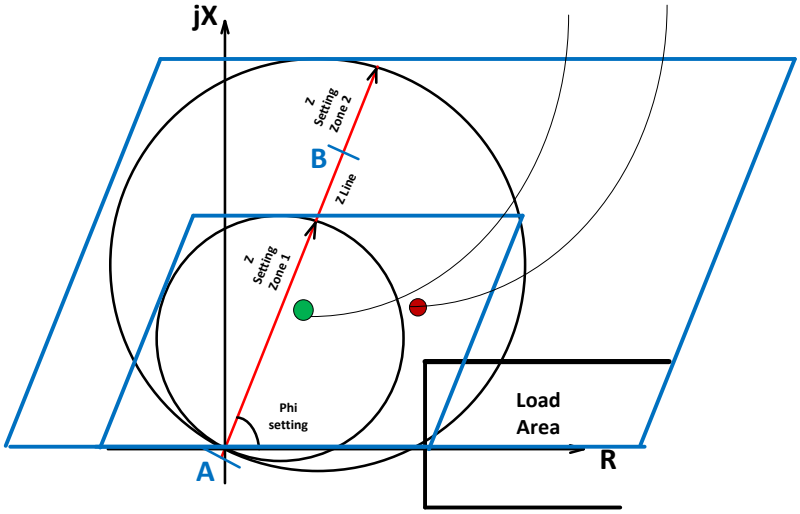

Figure 2.6 Mho and quadrilateral impedance characteristics

Impedance reach detection is determined by two types of characteristics shown in Figure 2.6. For line-to-line faults Mho characteristic is used while for all ground faults quadrilateral or polygonal characteristic is utilized.

The major advantage of polygonal characteristic is the possibility to detect high-impedance fault which can include high resistance part and deviate impedance reach from original point to the right. It is represented in the Figure 2.6 where impedance green point is shifted to the impedance red point on the value equal to resistance of fault.

3. PV Model and Grid Code

3.1 Introduction

PV model is essential part of the benchmark system. The PV array block has quite complex mathematics behind which should be explained in details.

Also it is control logic of grid-side inverter which defines the behaviour of PV plant during the fault conditions. For relay study it is important to know how this logic operates and how to control PV output behaviour.

The requirements which must be fulfilled by PV facility interconnected with main electrical system are defined by technical specification also called grid code which can vary from country to country. Main requirements related to this research are discussed more deeply in this chapter.

3.2 PV Model: The large time-step blocks

RSCAD model of PV plant consists of PV array with controlled insolation and ambient temperature input variables and capacitor for smoothing of voltage signal in the output as shown in Figure 3.1.

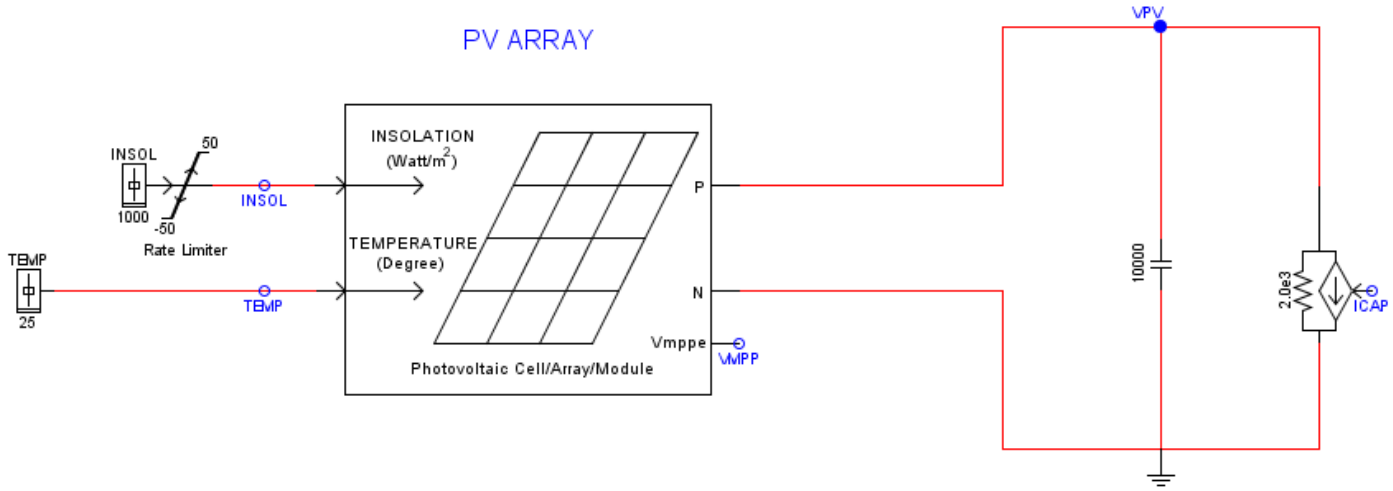

Figure 3.1 PV plant model in RSCAD

PV array consists of several solar cells from semiconductor material. Main advantage of this material is that it can produce electrical energy from sunlight. Solar cells are assembled in PV modules and then modules are creating PV arrays. Depending on type of cells, modules and arrays connection (parallel or series) output voltage and current from PV plant can be different.

Based on description in [17] an ideal solar cell is electrically represented as a current source in parallel with a single diode; however practical solar cell models require additional elements to accurately represent their nonlinear current-voltage characteristics. Thus, RSCAD model represent the solar cell with a series and shunt resistance as indicated in Figure 3.2.

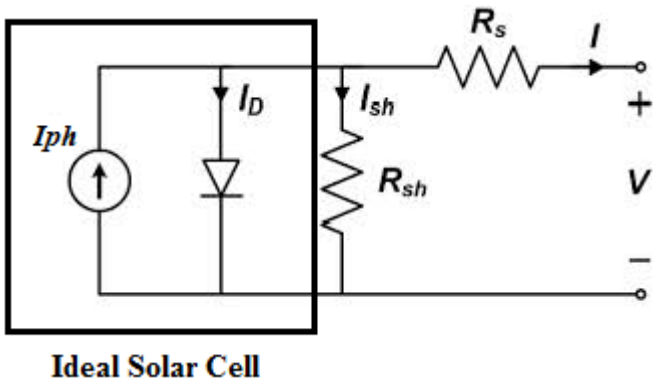

Figure 3.2 Single diode, five parameter model [17]

The single diode, five parameter model is simulated by equations 3.1 and 3.2 below.

$$I = I_{ph} - I_D - I_{sh} \tag{3.1}$$

$$I = I_{ph} - I_0 \cdot \left(\frac{\exp(V + R_S)}{N_S \cdot a \cdot V_t} - 1\right) - \frac{(V + R_S \cdot I)}{R_{sh}} \tag{3.2}$$

In order to make PV module to operate with the maximal power output the voltage is enforced to be at the Maximum Power Point (MPP). Also MPP depends on the ambient conditions like solar irradiance and ambient temperature. As described in [18] the I-V and the P-V characteristics shown in Figure 3.3 can be affected by fluctuations in ambient conditions. MPP will be moved correspondingly to these changes. For this purpose Maximum Power Point Tracking (MPPT) was designed which considers temperature and irradiance and keeps output power of PV module always in MPP.

The RSCAD PV model is using Lambert function approximation for MPPT and the expression 3.3 for it is given by [19] and shown below:

$$V_{mp} = V_{im} - \left(I_{im} - \frac{V_{im}}{R_{sh}}\right) \cdot R_S \tag{3.3}$$

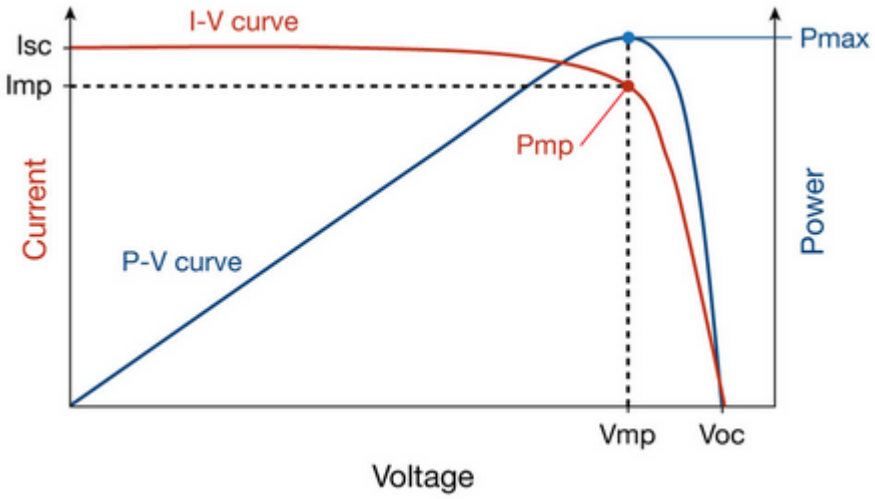

Figure 3.3 I-V and P-V curve of a solar cell [18]

3.3 PV Model: The small time-step blocks

Small time-step is necessary for more precise power electronic operation simulation. The commutation frequency of Voltage Source Converter (VSC) valves is around 20 kHz. This produces an issue if it is simulated in normal time step (~50μS). To faithfully represent the operation of the converters a small time step hierarchical box is used with a time step equal to 1400ns. The small time-step structure of the PV model consists of several elements in Figure 3.4. They are grouped in colour blocks depending of the task they perform.

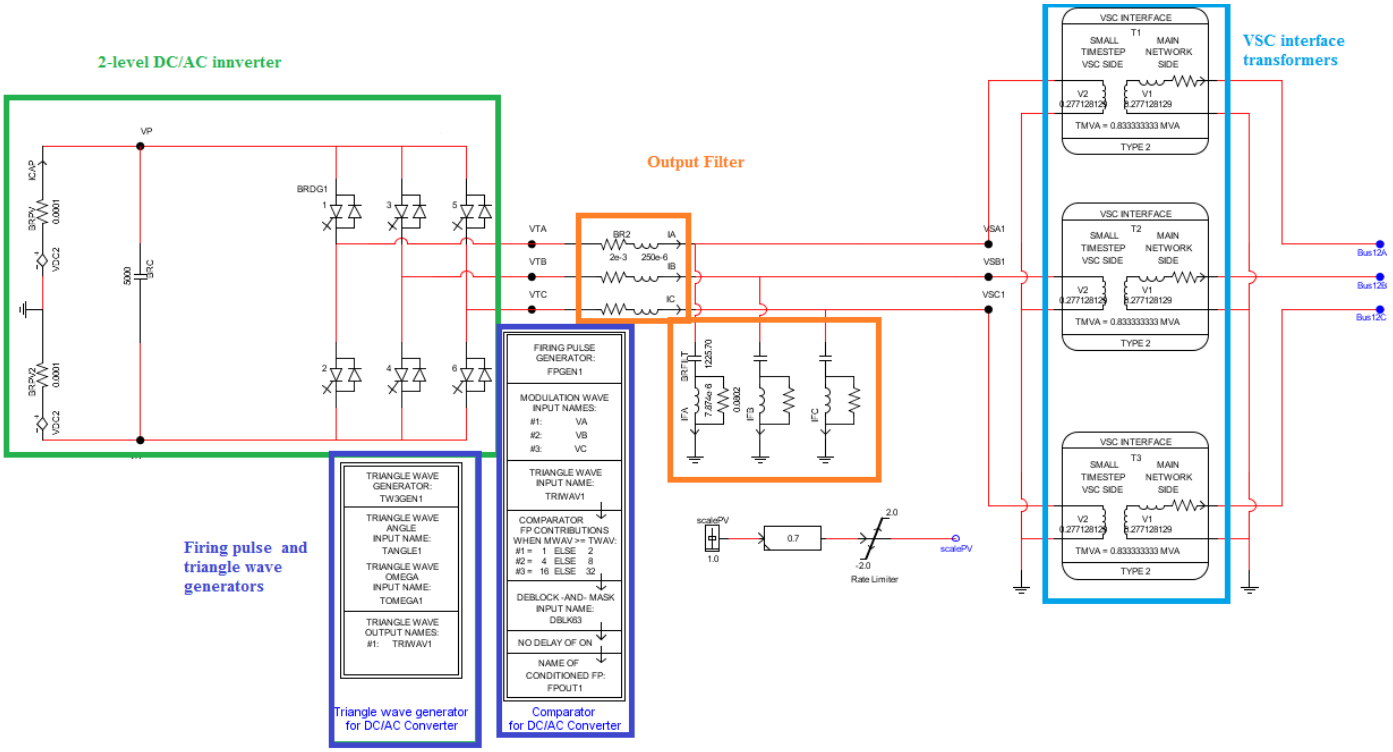

Figure 3.4 Small time-step blocks of PV model

There are 5 blocks inside:

1) 2-level DC/AC inverter which is used for conversion voltage and current from DC to AC.

2) Triangle wave generator which is necessary for pulse-width modulation (PWM) in firing pulse generator

3) Firing pulse generator for creation of signals for IGBTs in DC/AC inverter for switching

4) Output filter for elimination of higher harmonics and other signal distortions

5) VSC interface transformers for sending of signal from small time-step to large time-step blocks

In this way the PV plant model achieved an accurate performance during steady and transient's state conditions. It allows studying all spectres of frequencies in input energizing quantities.

3.4 PV Model: Control modules

According to Figure 3.5 general control logic consists of several stages:

1) Measurements of voltage and current in the point of current coupling

2) Outer controllers loop using grid side AC values and DC values from PV to provide reference currents for Inner controllers at the output

3) Inner controllers loop providing voltage reference wave for Modulator or Firing Pulse generator by comparison of current references and predefined by user current settings

4) Modulator which compare triangular wave and voltage references waves to create firing pulses for Inverter

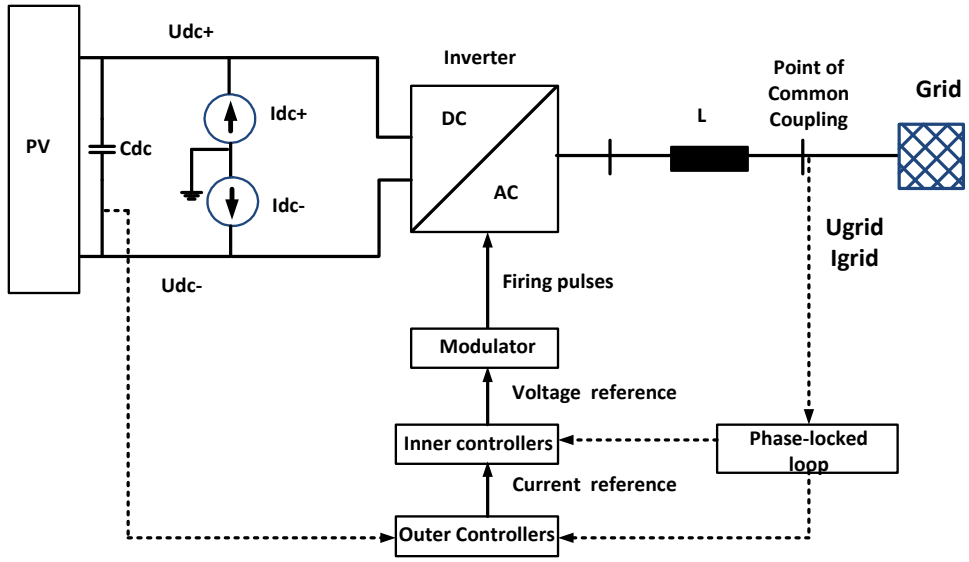

Figure 3.5 Generic function block diagram of grid-connected PV

Let's consider each component of PV inverter controls in details.

The first stage of control signal path is voltage and current decomposition as represented in Figure 3.6. In this PV model double synchronous reference control system was implemented for decoupled control of positive and negative sequence current which was suggested in [20] and tested in [21].

The following equations are used for decomposition of currents:

$$I_{\alpha pos} = \frac{1}{2} \cdot (I_{\alpha} + I_{\beta 90}) \tag{3.4}$$

$$I_{\alpha neg} = \frac{1}{2} \cdot (I_{\alpha} - I_{\beta 90}) \tag{3.5}$$

$$I_{\beta pos} = \frac{1}{2} \cdot (I_{\beta} - I_{\alpha 90}) \tag{3.6}$$

$$I_{\beta neg} = \frac{1}{2} \cdot (I_{\beta} + I_{\alpha 90}) \tag{3.7}$$

Decoupled positive and negative sequence improves output control signals by cancelation of the second harmonic.

ABC to *dq* transformation is necessary due to the fact that Proportional-Integral-Derivative (PID) controllers are working better with DC signals.

The second stage of signal path includes phase-locked loop (PLL) transformation.

The use of PLL constantly aligns the rotating *dq* reference to the voltage vector and provide decoupled active and reactive power control.

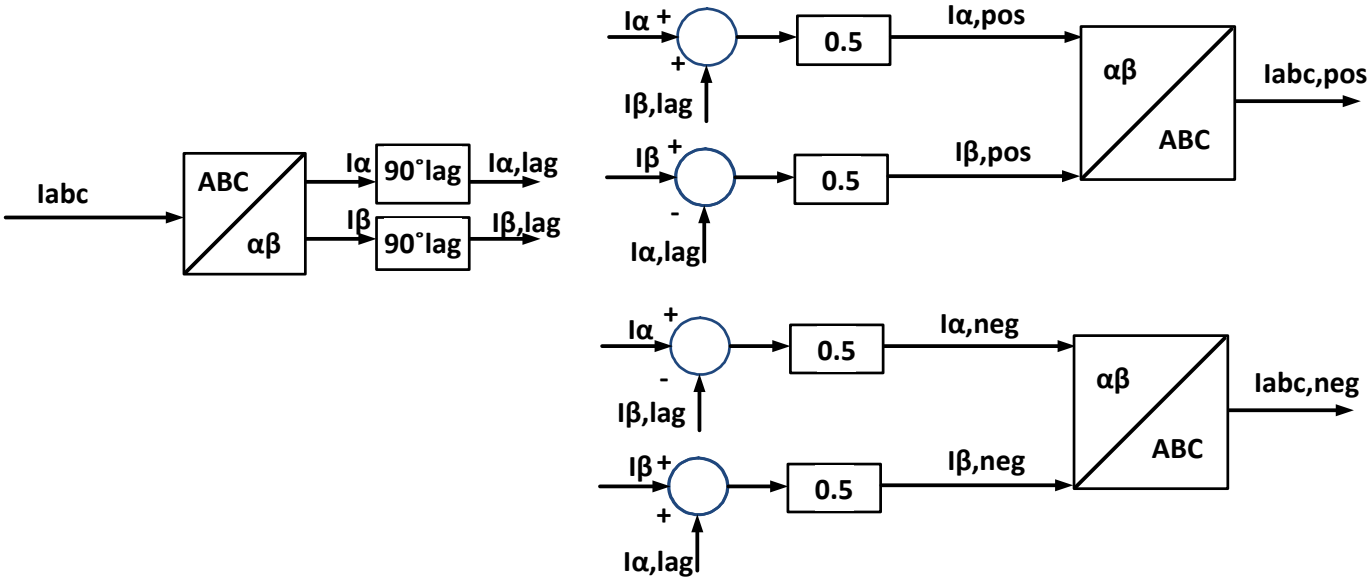

Figure 3.6 Current decomposition in positive and negative sequence

Inside PLL-T2 block the ABC to αβ transformation happens and PI controller with gain k=500 and T=0.01s is used to stabilize signal during any disturbances in the grid. The most important output signal is the angle angPLL which is necessary for correct *dq* transformation where Uq component is always zero.

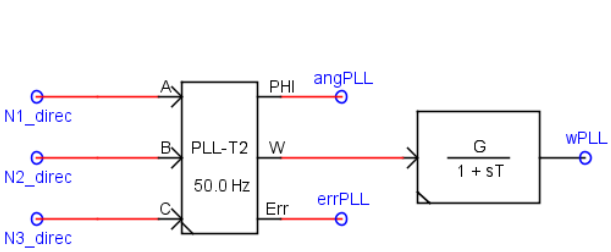

rtds_sharc_ctl_PLLT2

Parameters

Name	Description	Value	Unit	Min	Max
Frat	Base Frequency	50.0	Hz		
Ainit	Initial angle	0.0	deg	-360.0	720.0
PIPG	PI-Regulator Proportion Gain	500		0.0	
PIIT	PI-Regulator Integral Time Constant	0.01	sec	1.0e-6	
Ft	Filter Time-Constant	0.0015	sec	1.0e-6	
WMON	Monitor Omega?	rad/sec			
EMON	Monitor Error Signal?	Yes			
Proc	Assigned Controls Processor	6		1	36

Figure 3.7 PLL settings in RSCAD

Based on equations 3.8-3.11 the decoupled power control is implemented:

$$P = u^q \cdot i^q + u^d \cdot i^d \tag{3.8}$$

$$P = u^q \cdot i^d - u^d \cdot i^q \tag{3.9}$$

$$P = u^d \cdot i^d \tag{3.10}$$

$$P = -u^d \cdot i^q \tag{3.11}$$

The third stage of signal is outer control loop. For active power the DC voltage of PV is used as an input and compared with reference voltage from MPPT as shown in Figure 3.7.

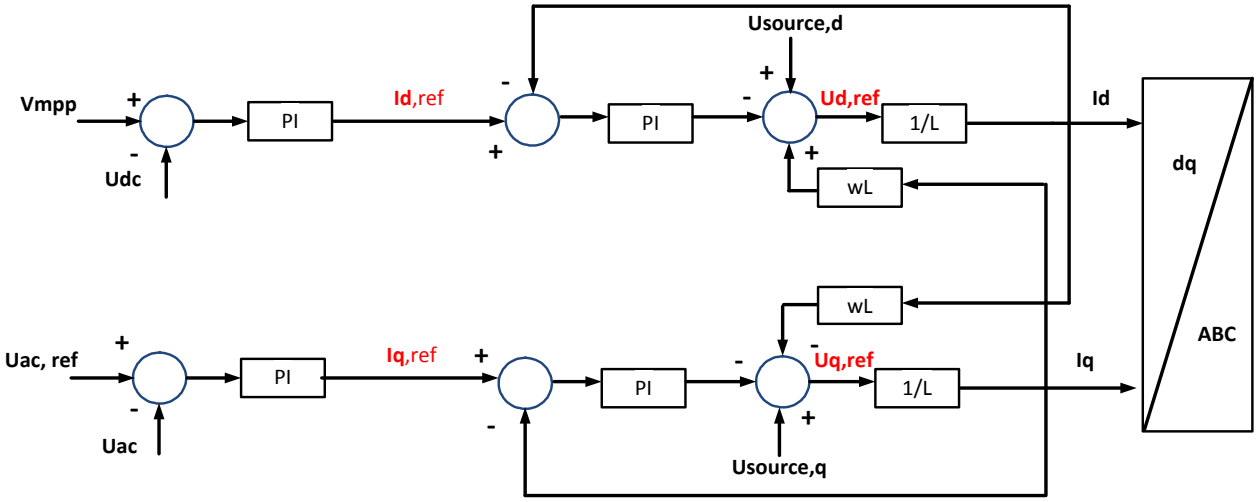

Figure 3.8 Outer and inner loops for active and reactive power

Reference currents *Id,ref* and *Iq,ref* calculated in outer loops are used as an input for inner loops. These signals are compared with values *Id* and *Iq* received from current decomposition.

The logic in inner loop can be described by following equations and is also shown in Figure 3.8.

$$i_d = \frac{u_{conv.d} - u_{source.d} + wLi_q}{sL} \tag{3.12}$$

$$i_q = \frac{u_{conv.q} - u_{source.q} - wLi_d}{sL} \tag{3.13}$$

In order to provide voltage support during fault conditions creating voltage dip more than 0.9 p.u. reactive current must be injected according to grid code. Fault ride-through strategy which gives a priority to reactive current was applied in PV controls and based on the logic which allows positive reactive current to be injected to a certain limit in compliance with grid code and characteristic shown in Figure 3.11 while positive active current injection is assigned to take the rest available capacity of reactive power. By this strategy converter is protected from over-loading of IGBTs. Logic for calculation of grid code references is represented in Figure 3.9.

Depending on the value of *fault_deep* signal reactive current *I_reac* is calculated. The same *I_reac* is used for calculation of active current reference in order to prevent over-loading of switches.

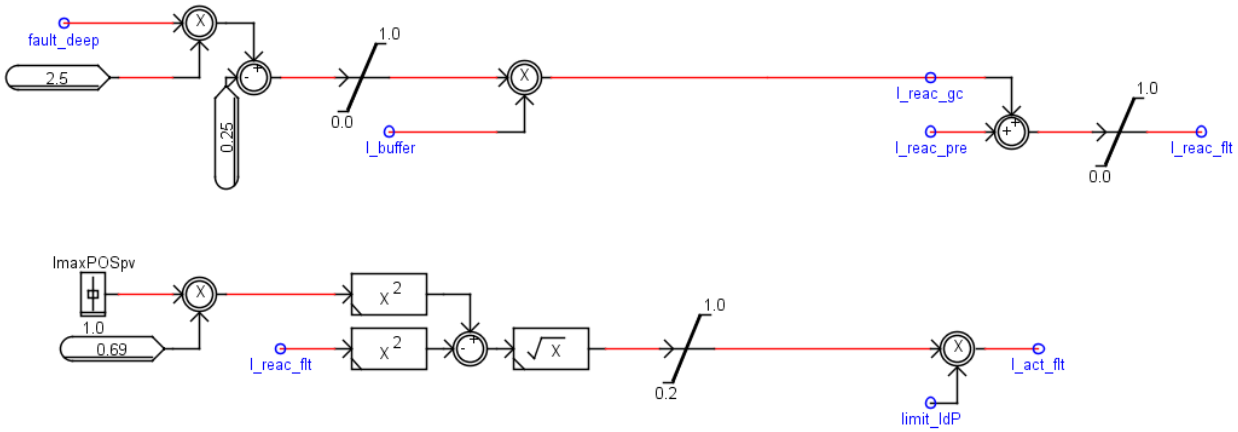

Figure 3.9 Logic for grid code references

One type of fault ride-through strategy was considered in this Master Thesis. The negative sequence current injection level is proportional to the negative sequence voltage level $I_{ref}(q,d)=k*V_{ref}(q,d)$ [20]. After inner loop the signal is transformed back to ABC components from *dq* and is sent to modulator.

In the final stage the modulator is creating firing pulses by comparison of triangular wave and reference signals V_a, V_b, and V_c appeared as an output from inner loop.

3.5 Grid Code

According to Tennet Grid Code which is used in Netherlands and Germany [16] all generation units are divided in two types. Type 1 generation plant is conventional synchronous generation unit directly connected to the grid or via transformers. Type 2 generation plant consists of the other generation units typically connected via power electronics. As a conclusion, large-scale PV plant is referred as type 2 generation facility.

For relay protection study the most important part of grid code is the behaviour of Type 2 generation plant during the event of faults in the grid. It is required that during fault conditions in the grid, generation plant should not be disconnected from the grid. The disconnection time is defined according to characteristic shown in Figure 3.10.

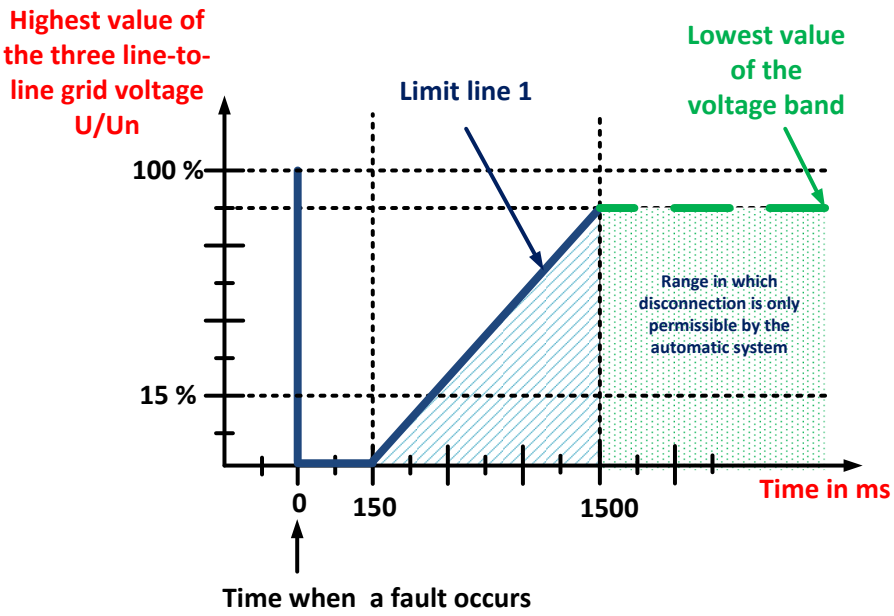

Figure 3.10 Fault Ride-Through characteristic

If the voltage drop at the point of common coupling is lower than limit line 1 shown in the Figure 3.10 then a quick disconnection of generation plant is allowed.

PV plant must provide reactive current support during fault condition also called fault-ride-through requirement. In acceptance to Figure 3.11 the fault ride-through requires that during fault condition when voltage varies more than 10% of nominal value the renewable intermittent source must provide reactive current output shown by red line in Figure 3.11 below. If the voltage is 10% less than nominal the low voltage ride-through characteristic is applied, otherwise high voltage ride-through characteristic is used. Renewable intermittent sources must support grid voltage during all types of fault with not only positive but also negative short-circuit reactive current injections.

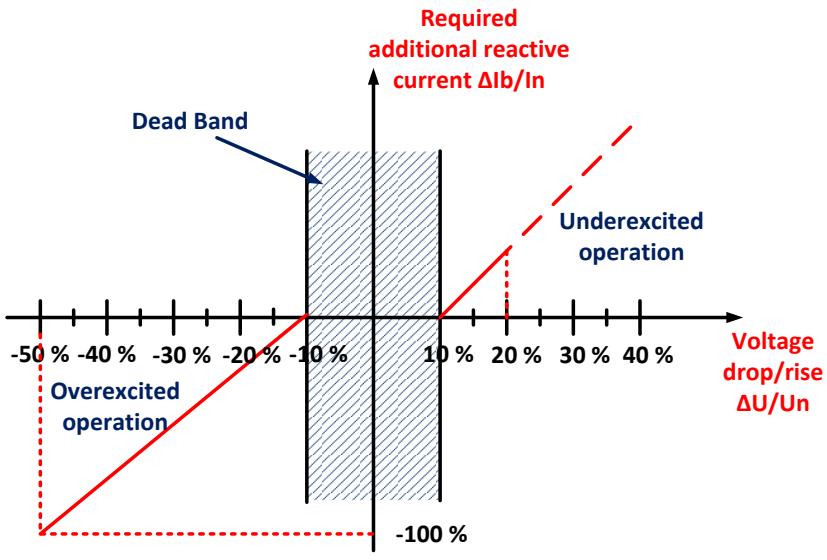

Figure 3.11 Reactive current support

In case of more serious voltage dip the renewable sources must be disconnected from the grid for stability of the system.

After voltage level is recovered to nominal value and stay in the dead band area the voltage support must be provided in extra 500 ms and the transient balancing procedures following the voltage return must be completed after 300 ms based on [16].

Due to the fact that renewable sources must be connected for some time during fault condition the current level which is injected by PV plants is important to observe in order to avoid problems in protection maloperation.

In grid protection section Tennet Grid Code stated that at least a distance protection relay must be installed at all grid connection points [16].

Due to the fact that in this research 400 kV extra high-voltage transmission line will be considered next regulations are applied to protection devices:

1) Fault must be cleared in less than 150 ms.

2) Selectivity of the device must be 100%

3) Single-phase automatic reclosure must be fulfilled on overhead lines with an interval of 1 to 1.2 seconds

4) Circuit breaker failure protection system

For proper research of current flowing during faults occurrence electromagnetic transient software must be used to be able to consider all set of frequencies and travelling waves effects in the system. Thus, the model of system for study of current effect was developed in RSCAD which enables transient study.

4. Test System Model

4.1 Introduction

The benchmark model for testing was designed in a way to investigate the distance protection function operation under several scenarios. In order to be able to check all test scenarios the benchmark model must have a number of specific features.

It must:

1) give a possibility to switch between weak grid and strong grid,

2) allow connection of PV plant with different generation capacity,

3) enable fast connection and disconnection of conventional plant and PV plant,

4) be easily replicated and have parameters accessible in open sources.

4.2 Model Topology

The benchmark model for testing was based on the two areas grid topology from [22] and is depicted in Figure 4.1. The system enhanced further to meet requirements for the specified analysis of distance protection. Parameters for the lines, loads, and generators were taken from [22] and expressed in per unit values.

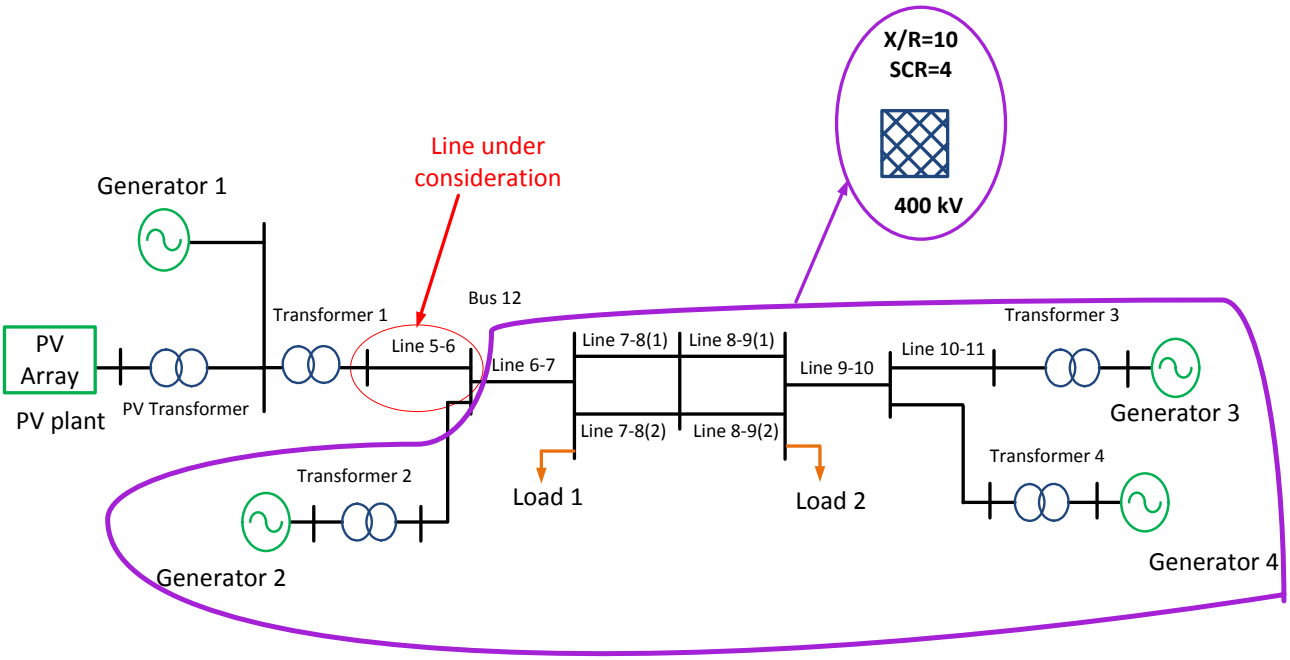

Figure 4.1 Topology of enhanced Khundur system

In the first step of this research, the test system was modelled in DigSILENT Power Factory in order to obtain power flow results. It was implemented in Power Factory because the interface for power flow

analysis is user friendly in DigSILENT and effect of any changes in the grid was easily visualized as represented in Figure 4.2. By this step initial conditions for generators in RSCAD were defined to get correct power flow through line under consideration in the steady-state conditions.

The initialization of generators is comprised of two parameters:

1) Voltage magnitude

2) Voltage angle

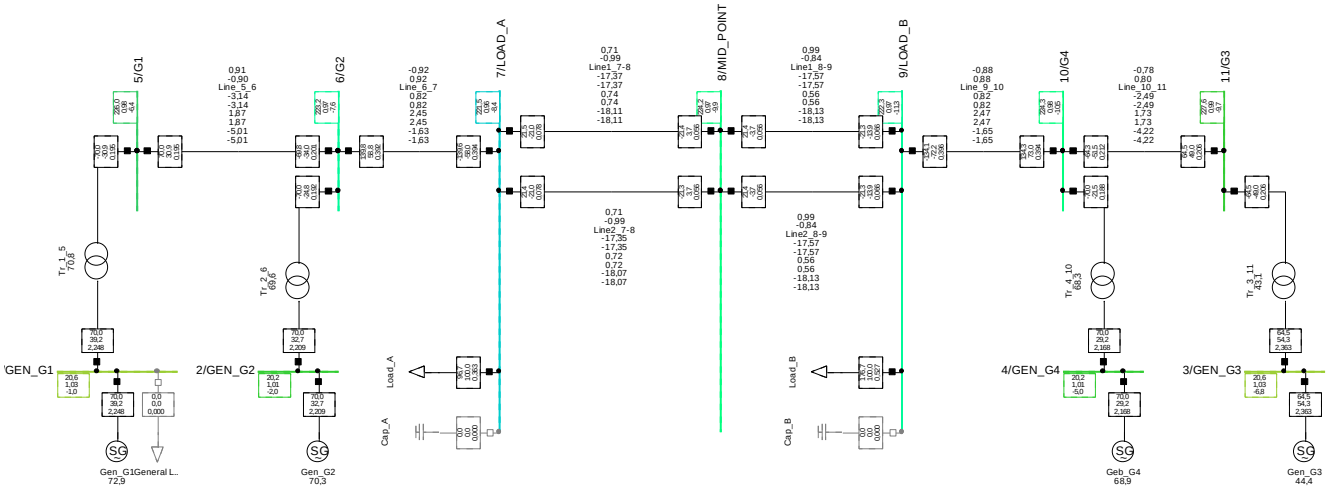

Figure 4.2 Power Factory model and Power flow analysis

In the second step, the same model was recreated in RSCAD. In order to validate the correctness of the model a set of simulation was conducted in steady-state and transient mode. RSCAD internal function for power flow enables to compare voltage amplitude and angle in each bus in the grid with Power Factory results as shown in Figure 4.3.

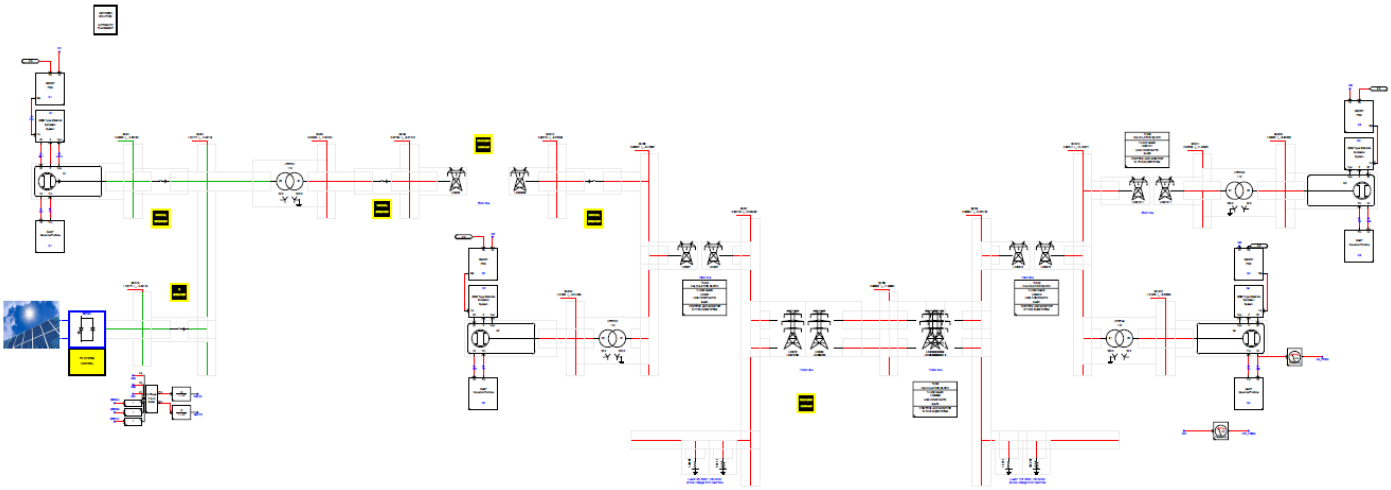

Figure 4.3 RSCAD initial model

4.3 Short Circuit Ratio

In order to make the benchmark model more compact and flexible for PV plant controllers tuning the part of the grid on the right from line under consideration was replaced by equivalised source. The concept of short circuit ration (SCR) was used to get the same fault current behaviour. Short circuit ratio of AC system is very useful for measurement of strength of system. It is even more important to consider SCR in systems with combinations of AC and DC lines. By SCR we can identify if the system is weak or strong and it is also essential for tuning of PID controllers of power electronic devices.

According to [22] the formulas and typical values of SCR are mentioned below.

$$SCR = \frac{short-curcuit\_MVA\_of\_AC\_system}{DC\_converter\_MW\_rating} \tag{4.1}$$

The short-circuit MVA is given by

$$SCMVA = \frac{Eac^2}{Zth} \tag{4.2}$$

where *Eac* is the commutation bus voltage at rated DC power and *Zth* is the Thevenin equivalent impedance of the AC system.

Traditionally the AC system strength has been classified as follows.

1) High if SCR is greater than 5.

2) Moderate if SCR is between 3 and 5.

3) Low if SCR is less than 3.

SCR in the bus 12 in Figure 4.1 during 100 MVA PV plant connections is equal to 4. That is why, the short circuit contribution of three-phase equivalent voltage source must have the same output value. Based on theory described above the values of impedance magnitude and impedance angle were calculated. X/R ratio is equal to 10 in this case.

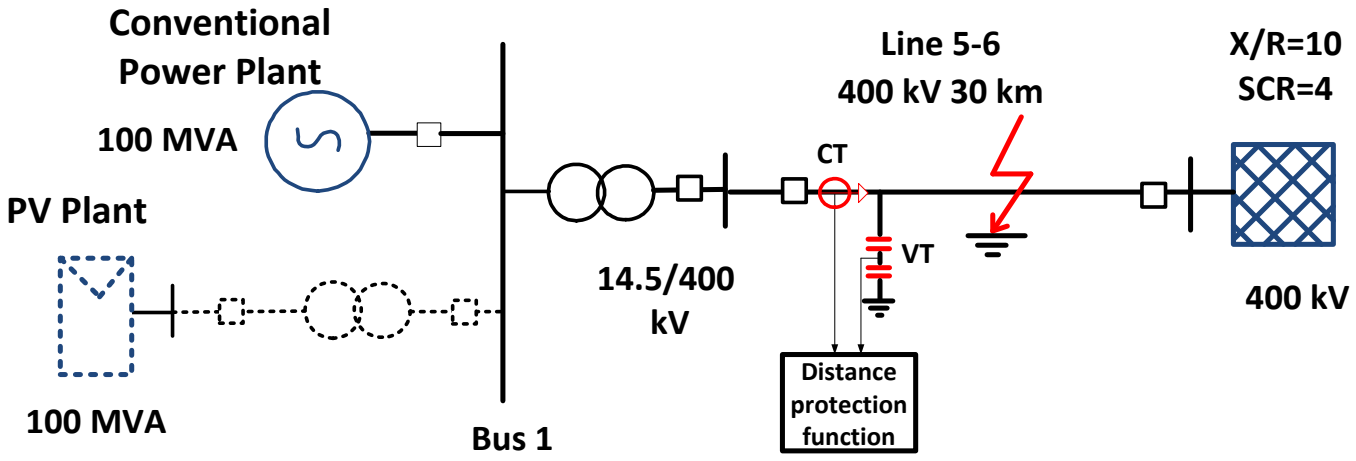

Figure 4.4 Topology of grid with equivalised source in RSCAD

PV model described in previous chapter was connected to the grid at the same bus as generator named “G1” from the left side of the line under consideration. Two circuit breakers were created to enable two cases: only synchronous generator connection and only PV connection in the end of the radial line as shown in the Figure 4.4.

4.4 Overhead Line and Fault Logic

Line under consideration is 30 km, 400 kV overhead (OHL) line. The Bergeron model of OHL was used for detailed simulation of line parameters frequency dependence and travelling wave effect. The OHL parameters are shown in Table 4.1. In order to use value of fault distance as variable, two Bergeron model blocks were used.

Table 4.1 Parameters of the 400 kV line**.**

Sequence	R(Ohm/km)	XL(Ohnm/km)	Xc(MOhm*km)
Positive/Negative	0.02701	0.3087	0.2664
Zero	0.277	0.98475	2.664

Two blocks for interphase and phase-to-ground faults were implemented in test model as shown in Figure 4.5. The fault resistance variable is defined inside these two blocks to create high impedance fault. Logic in the Figure 4.6 is used to simulate all types of faults including line-to-ground, line-to-line, two lines-to-ground and balanced three-phase fault.

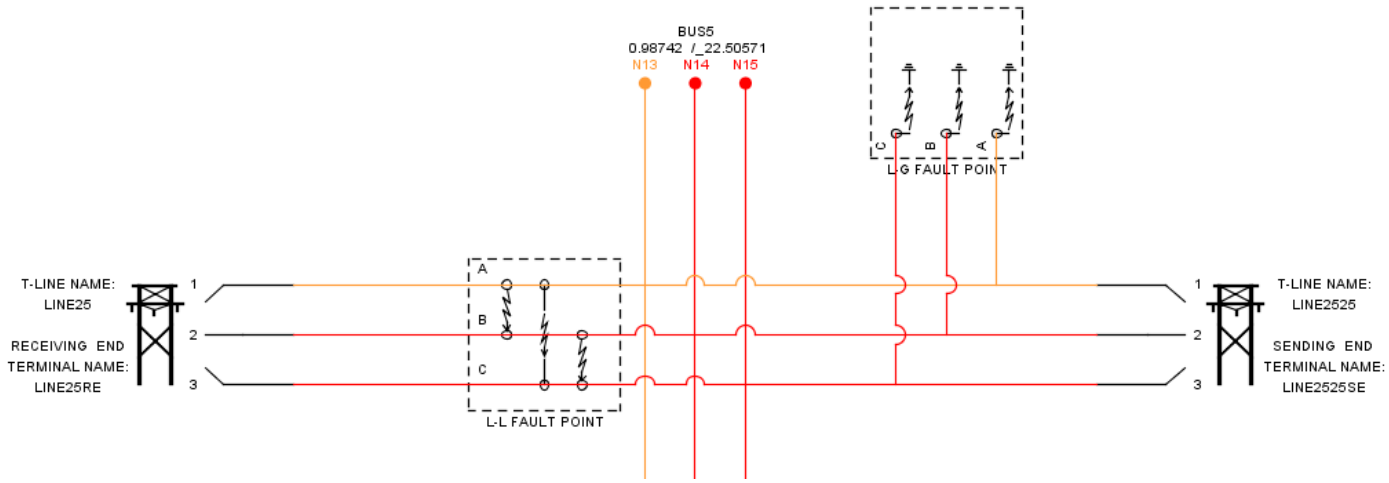

Figure 4.5 Fault in RSCAD model

Fault simulation is started with push button *PB1012* generating signal equals to 1. To create the fault in appropriate time the edge detector and comparator block are used which took the voltage wave as a reference and wait for zero voltage crossing. Next block after push button enables time delay of 0.02 seconds for injecting the fault at the peak of the voltage wave to create most extreme case of fault occurrence. After that the signal is going through slider block defining the duration of the fault *SL22*.

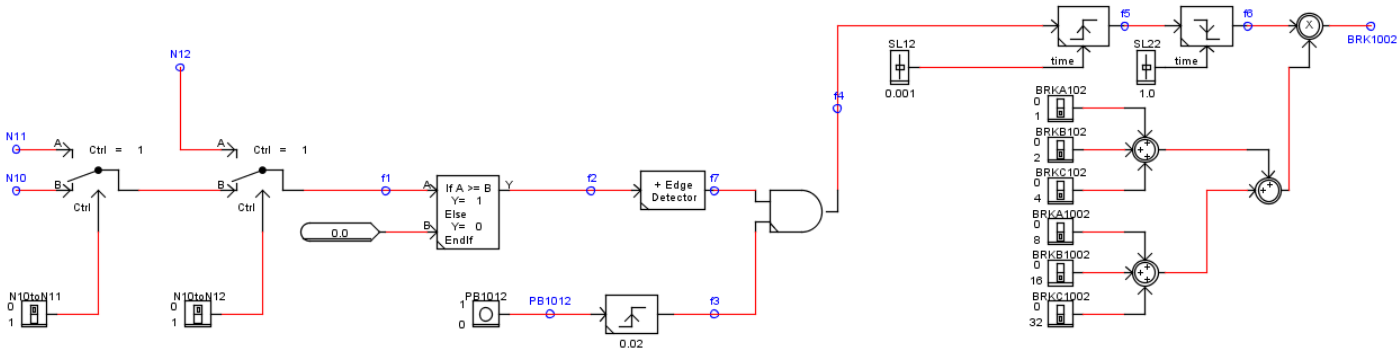

Figure 4.6 Fault logic

For correct operation of fault block six breakers were used. Each breaker was assigned to definite bit number 1, 2, 4, 8, 16 and 32. Signals from all breakers were summed up and multiplied by signal 1 coming from push button described earlier. In order to simulate three-phase or two lines-to-ground fault the bit number of all breakers must be correlated to create correct binary signal in the output.

4.5 Synchronous Generator

Generator parameters represented in Table 4.2 were taken from [22]. Apparent power of synchronous generator was 170 MVA. The governor models of type GAST in combination with gas turbine and excitation system of IEEE Type ESAC4A were used to control turbo generator.

Table 4.2 Parameters of synchronous generator

Parameter		FBM (p.u)
Stator leakage inductance	*Xl*	0.2
Synchronous reactance	*Xd*	1.80
	Xq	1.70
Transient reactance	*X'd*	0.30
	X'q	0.55
Subtransient reactance	*X''d*	0.25
	X''q	0.25
Transient OC time constants	*T'd0*	8.00
	T'q0	0.40
Subtransient OC Time constants	*T''d0*	0.03
	T''q0	0.05

In this generator model following specification are applied:

1) Space and slot harmonics are not considered.

2) Magnetic saturation effect is incorporated.

3) Torque and speed are monitored in per unit values.

4) When the speed is positive, positive electric torque corresponds to generating operation of the machine and negative electric torque corresponds to motoring operation of the machine [23].

As indicated in Figure 4.7, the synchronous generator is modelled in combination with two blocks governor and exciter.

Exciter is tracking voltage level in generator *Vpu* and value of excitation current *If* in order to provide control of field voltage *Ef.* Governor is tracking rotor speed for control of mechanical torque value in the input of generator.

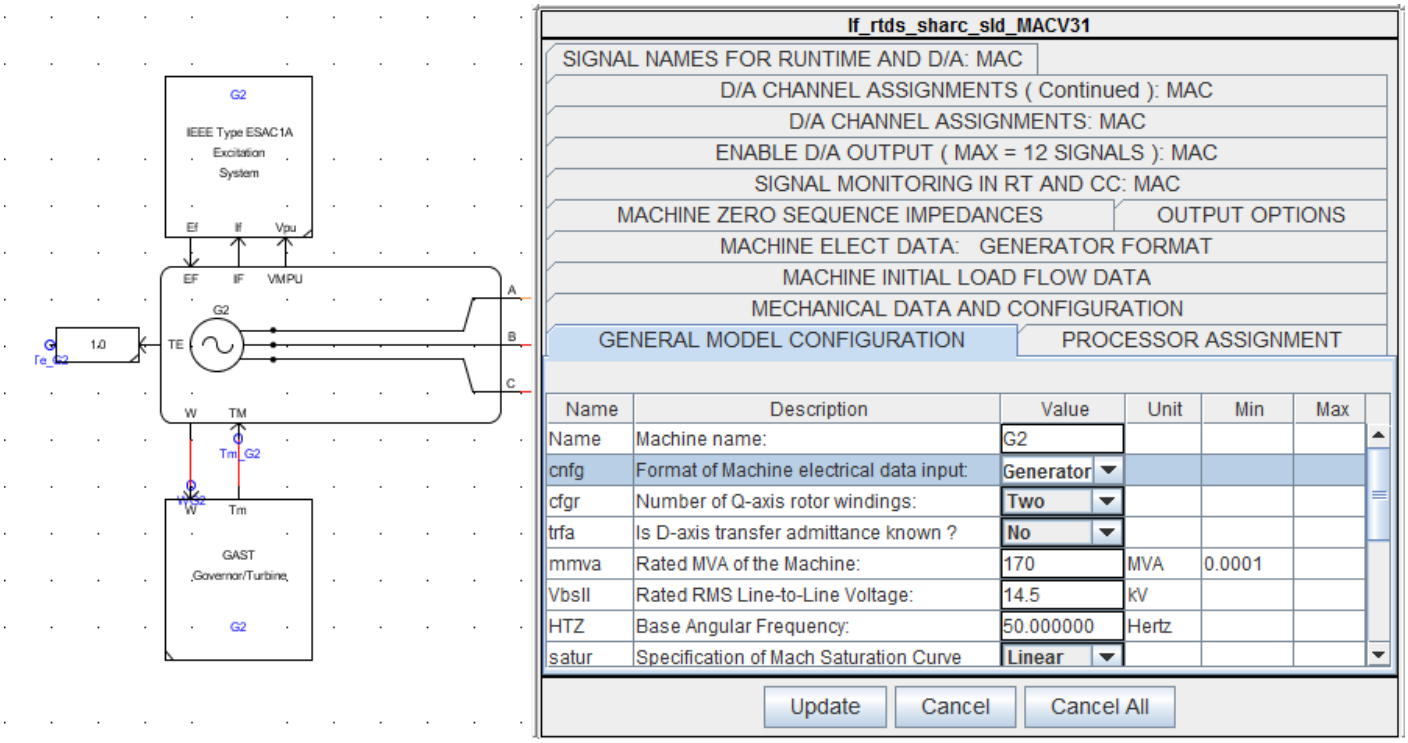

Figure 4.7 Synchronous generator model in RSCAD

5. Hardware-in-the-loop Test Setup

5.1 Introduction

Hardware-in-the-loop test setup comprises RTDS and consists of several stages.

The first stage is software modelling including processing of binary signals from breakers (breaker status signal) and analogical signals from current transformers and voltage transformers.

The second stage is a hardware connection of distance protection to Gigabit Transceiver Analogue Output (GTAO) and Gigabit Transceiver Front Panel Interface (GTFPI) cards via amplifiers.

And the final stage includes development of script for test automation and plotting in Matlab and verification of correct protection response on fault actions.

Functional block diagram of the hardware-in-the-loop test which indicates general concept of setup is shown in Figure 5.1. The detailed explanation of each block is provided in the following sections.

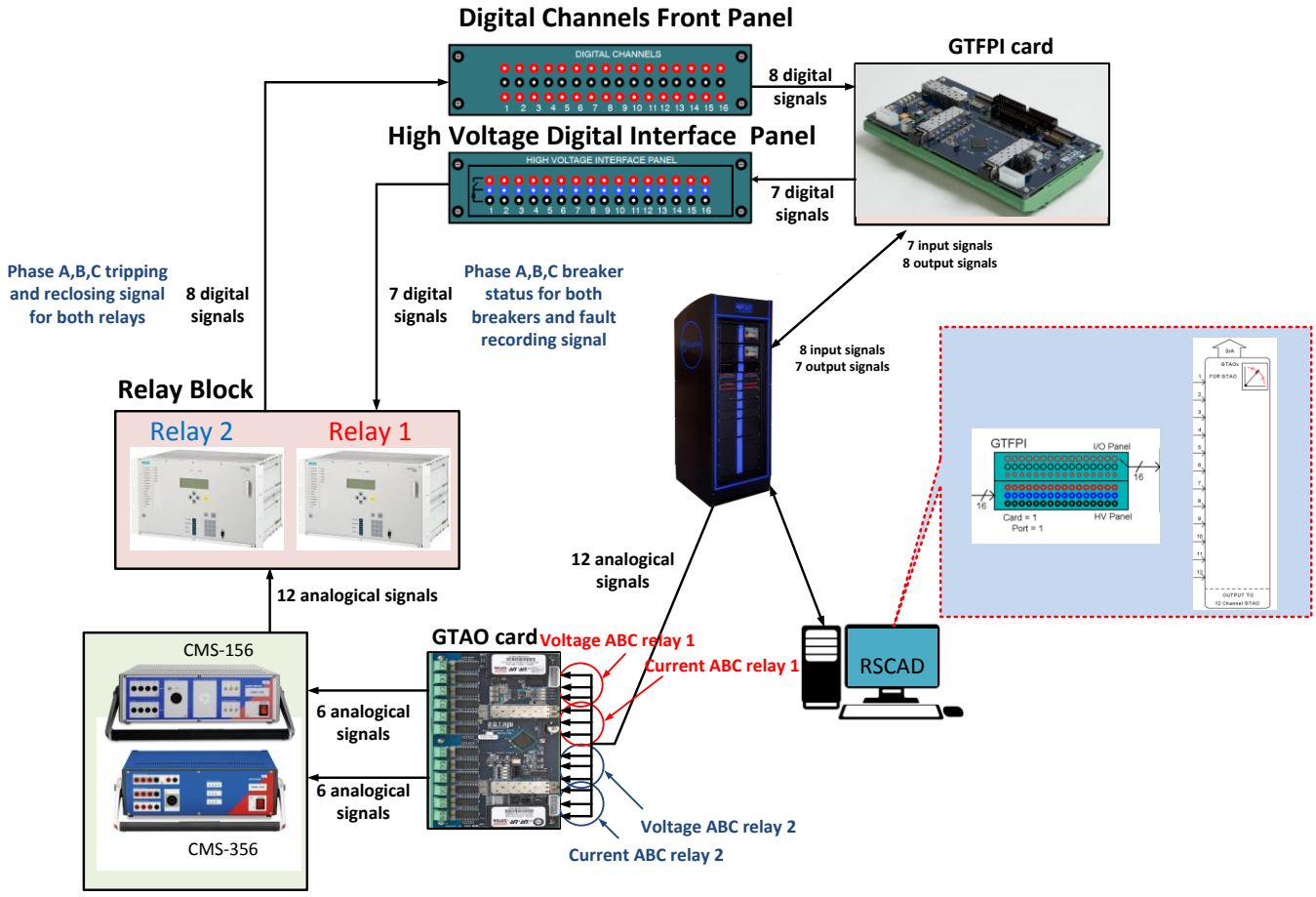

Figure 5.1 Function block diagram of hardware-in-the-loop test

5.2 Software Simulation

In order to send the analogical signals of currents and voltages from the benchmark system model in RSCAD to commercial relays and binary signals backward the special interface blocks Gigabit Transceiver Analogue Output (GTAO) and Gigabit Transceiver Front Panel Interface (GTFPI) shown in Figure 5.2 and Figure 5.3 are used.

Analogical signals from voltage transformer (VT) and current transformer (CT) of two relays are sent to GTAO card where output signal voltage is in range from -10 V to 10 V. As indicated in Figure 5.2, signals *N10, N11, N12* are referred to voltage phases A, B, and C from VT for the first relay, signals *IBURA40, IBURB40, IBURC40* are referred to currents from CT for the first relay, while signals *N34, N35, N36* and *IBURA4, IBURB4, IBURC4* are related to the second relay.

For safety reasons scaling factor is provided inside GTAO block to avoid overvoltage of GTAO card during transient conditions in the grid.

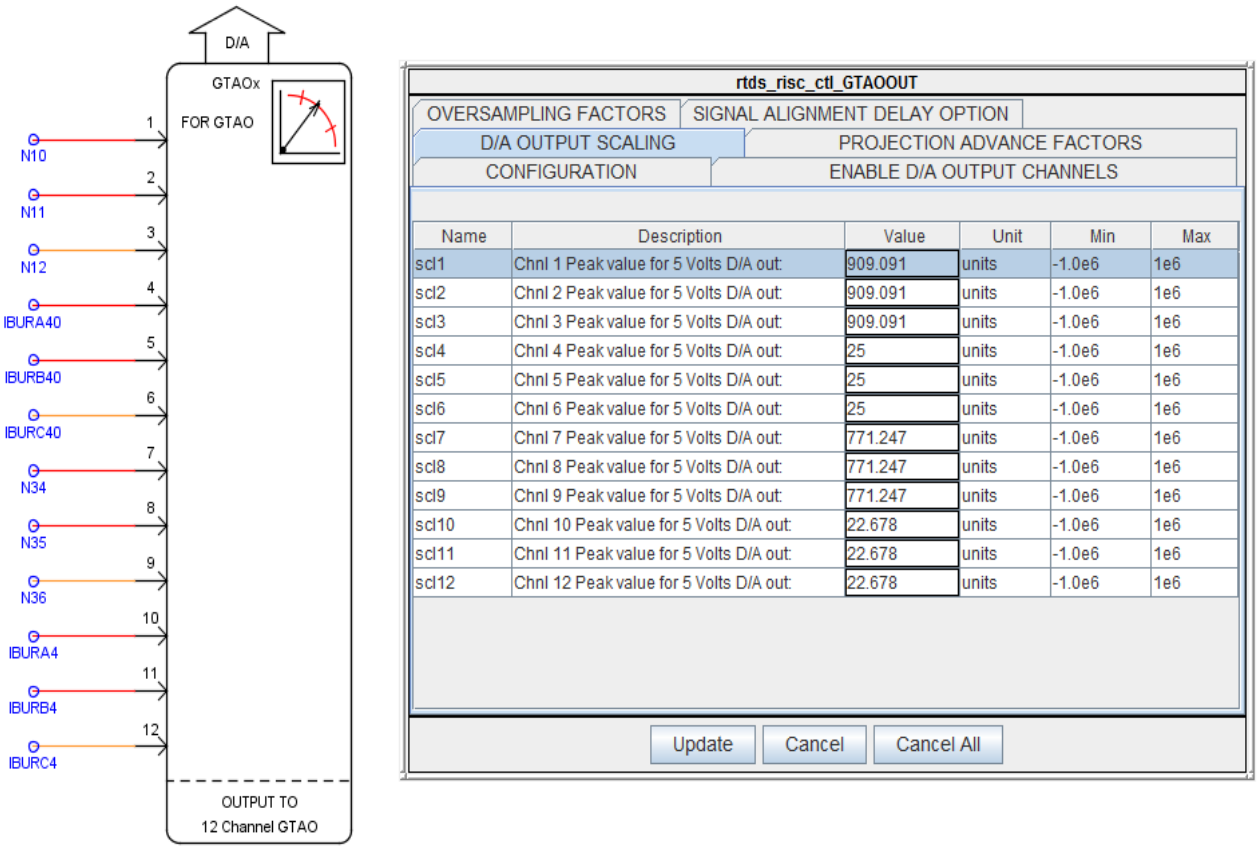

Name	Description	Value	Unit	Min	Max
scl1	Chnl 1 Peak value for 5 Volts D/A out:	909.091	units	-1.0e6	1e6
scl2	Chnl 2 Peak value for 5 Volts D/A out:	909.091	units	-1.0e6	1e6
scl3	Chnl 3 Peak value for 5 Volts D/A out:	909.091	units	-1.0e6	1e6
scl4	Chnl 4 Peak value for 5 Volts D/A out:	25	units	-1.0e6	1e6
scl5	Chnl 5 Peak value for 5 Volts D/A out:	25	units	-1.0e6	1e6
scl6	Chnl 6 Peak value for 5 Volts D/A out:	25	units	-1.0e6	1e6
scl7	Chnl 7 Peak value for 5 Volts D/A out:	771.247	units	-1.0e6	1e6
scl8	Chnl 8 Peak value for 5 Volts D/A out:	771.247	units	-1.0e6	1e6
scl9	Chnl 9 Peak value for 5 Volts D/A out:	771.247	units	-1.0e6	1e6
scl10	Chnl 10 Peak value for 5 Volts D/A out:	22.678	units	-1.0e6	1e6
scl11	Chnl 11 Peak value for 5 Volts D/A out:	22.678	units	-1.0e6	1e6
scl12	Chnl 12 Peak value for 5 Volts D/A out:	22.678	units	-1.0e6	1e6

Figure 5.2 RSCAD interface GTAO block and scaling factors

Let's consider the procedure of scaling factor calculation for voltages and currents of relay one. MathCAD software was used to automate calculations.

Firstly the ratio of voltage and current transformers are computed based on equations (5.1) and (5.2).

$$N_{VT} = \frac{V_{primary}}{V_{secondary}} \tag{5.1}$$

$$N_{CT} = \frac{I_{primary}}{I_{secondary}} \tag{5.2}$$

where $V_{primary}$, $V_{secondary}$, $I_{primary}$, and $I_{secondary}$ are taken from relay technical specifications.

In the relay logic the line-to-ground voltage and current values are converted into line-to-line values by multiplication on coefficient $\sqrt{3}$ which also must be taken into account.

Two amplifiers CMS-156 and CMS-356 are used in the hardware-in-the-loop setup. The ratio of amplifier must be considered for calculation of scaling factor. Voltage values received from GTAO card amplifier CMS-156 increases by 50 times and for currents values by 5 times. Technical data of CMS-156 amplifier is shown in appendix A.

CMS-356 amplifier is working with root-mean-square (RMS) values of voltages and currents so extra coefficient $\sqrt{2}$ is included in case of its application. For voltage values received from GTAO card amplifier CMS-356 is increasing by 60 times and for currents values by 6.4 times. Technical data of CMS-356 amplifier is also shown in appendix A.

Based on factors and coefficients mentioned above and the value of current or voltage which we expect to appear in the relay display (it should be the same as in RSCAD plots) the voltage of GTAO signal is calculated by equations (5.3) and (5.4) and later checked manually by multimeter at GTAO card.

$$V_{GTAO} = \frac{V_{L-L}}{\sqrt{3}} \cdot \frac{1}{N_{VT}} \cdot \frac{1}{N_{V\_AMP}} \tag{5.3}$$

$$V_{GTAO} = I_{L-N} \cdot \frac{1}{N_{CT}} \cdot \frac{1}{N_{I\_AMP}} \tag{5.4}$$

Extra coefficient of 5 is used inside GTAO block. Thus, the scaling factors value can be calculated based on equations (5.5) and (5.6)

$$Scaling\_factor1 = V_{L-N} \cdot \frac{5}{V_{GTAO}} \tag{5.5}$$

$$Scaling\_factor2 = I_{L-N} \cdot \frac{5}{V_{GTAO}} \tag{5.6}$$

The GTAO card is connected to a processor card via the Gigabit Transceiver Input Output port using a fibre cable. Overall 12 signals are received by two numerical relays for correct impedance calculation, six signals for each device.

Signals from digital relays are sent back to RSCAD GTFPI block shown in Figure 5.3 via High Voltage Digital Interface Panel and GTFPI card. Four signals include three trip signals for each phase (A, B, C) in the virtual breaker *phaAop2relay1, phaBop2relay1, phaCop2relay1* and one reclosing command *recloser2relay1*. As the result eight signals are provided by two relays and are sent to virtual breakers in RSCAD model.

These signals are sent to word-to-bit block for conversion from integer word to multiple logical signals. All output signals are binary either 0 or 1. The input signal is an integer. After these block a set of binary signals is obtained which enable virtual breaker switching.

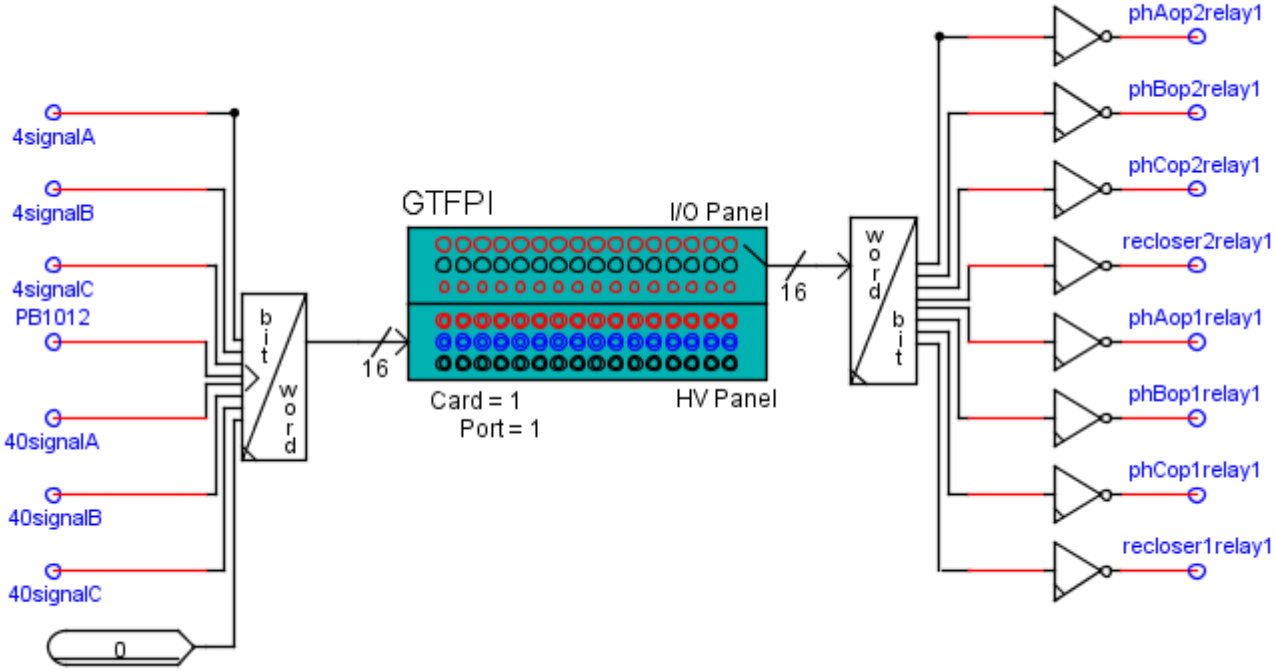

Figure 5.3 RSCAD interface GTFPI block

To enable manual switching of breakers a set of push-buttons was created as indicated in Figure 5.4. It consists of 8 buttons sending the signals to trip signal selection block. It is possible to close or open only one phase or all 3 phases of the breaker.

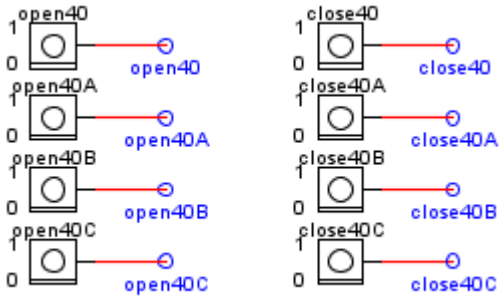

Figure 5.4 Breaker manual switching

The open or close signals are chosen from the number of options for example: *open40*, *open40A* and *phAop1relay1* shown in Figure 5.5. “Or” logical element is used to give a possibility to switch between these options.

Open40 is used for three phase manual open action.

Open40A is used for phase A manual open action.

PhAop1relay1 is used to switch breaker by binary signal from real device.

It is necessary for benchmark system model to have all three options in order to make it flexible and adapt to different test scenarios.

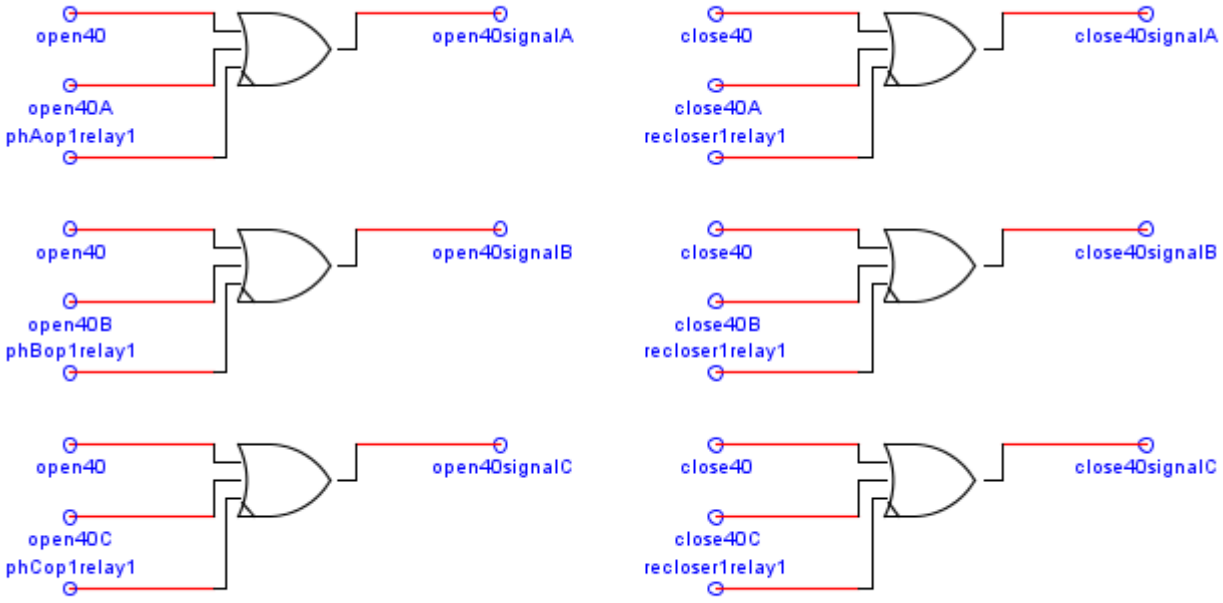

Figure 5.5 Trip signal selection

After that the signals for open and close actions are collected and sent to bit-to-word block where the combination of binary signals is recorded in integer word *BRK40*. This word is used in virtual breaker model and defines how breaker should operate.

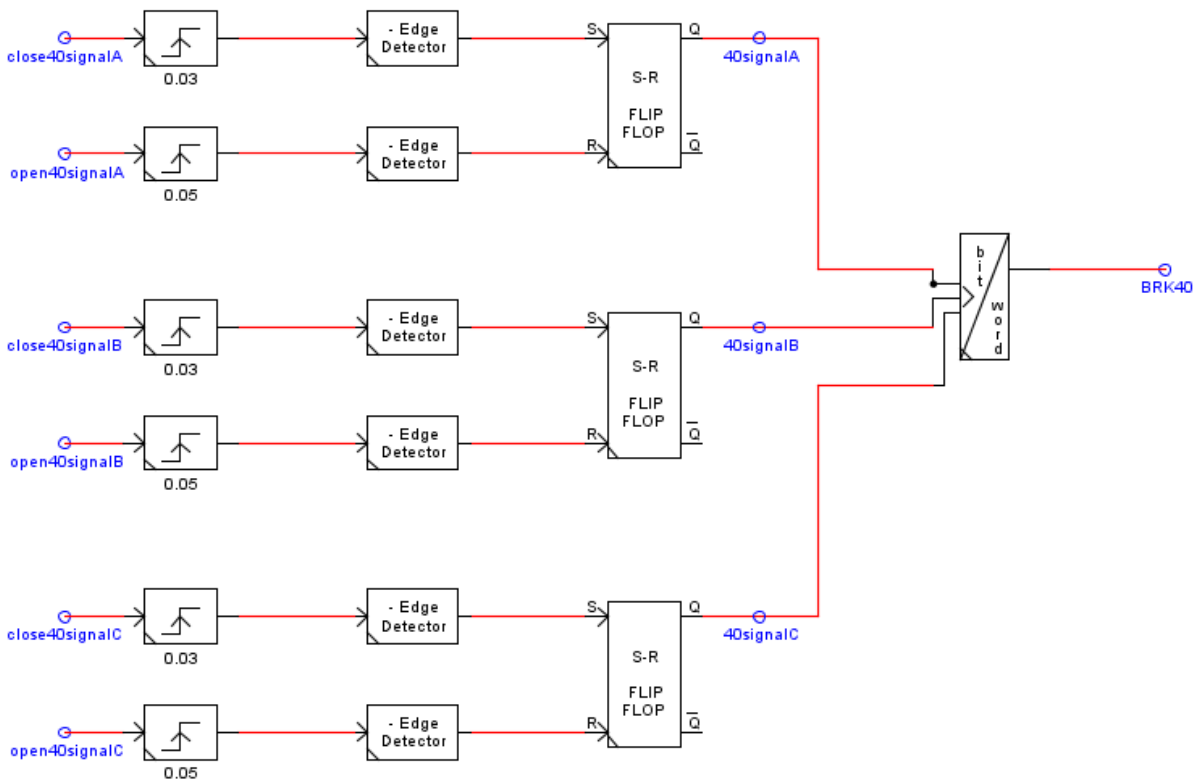

Figure 5.6 Trip signal processing

The signals of breaker status and signal for recoding of fault in the relay are sent back to relays after all previous actions via GTFPI block in RSCAD and High Voltage Front Interface Panel as shown in Figure 5.1. By this step the loop is closed and hardware-in-the-loop test can be conducted.

This step is made with the help of signals *40signalA*, *40signalB*, and *40signalC* shown in Figure 5.6. These binary signals define the state of breaker phases whether they are in open or closed state. These data is send to digital relay to know if it is possible to trigger or not.

One extra signal *PB1012* shown in Figure 5.3 is responsible for fault recording action in commercial numerical relay. It is created from push-button and linked to the start of fault. It is crucial to have this signal because it enables to record the waves of current and voltages and impedance reach during the fault if relay did not detect it.

5.3 Hardware Connections

The laptop with RSCAD software is connected to RTDS via internet by special router. The router is connected to PB5 processor cards hub with Ethernet cable. Thus, the RSCAD model saved in laptop is sent to processor cards of RTDS making possible fast real-time calculation speed.

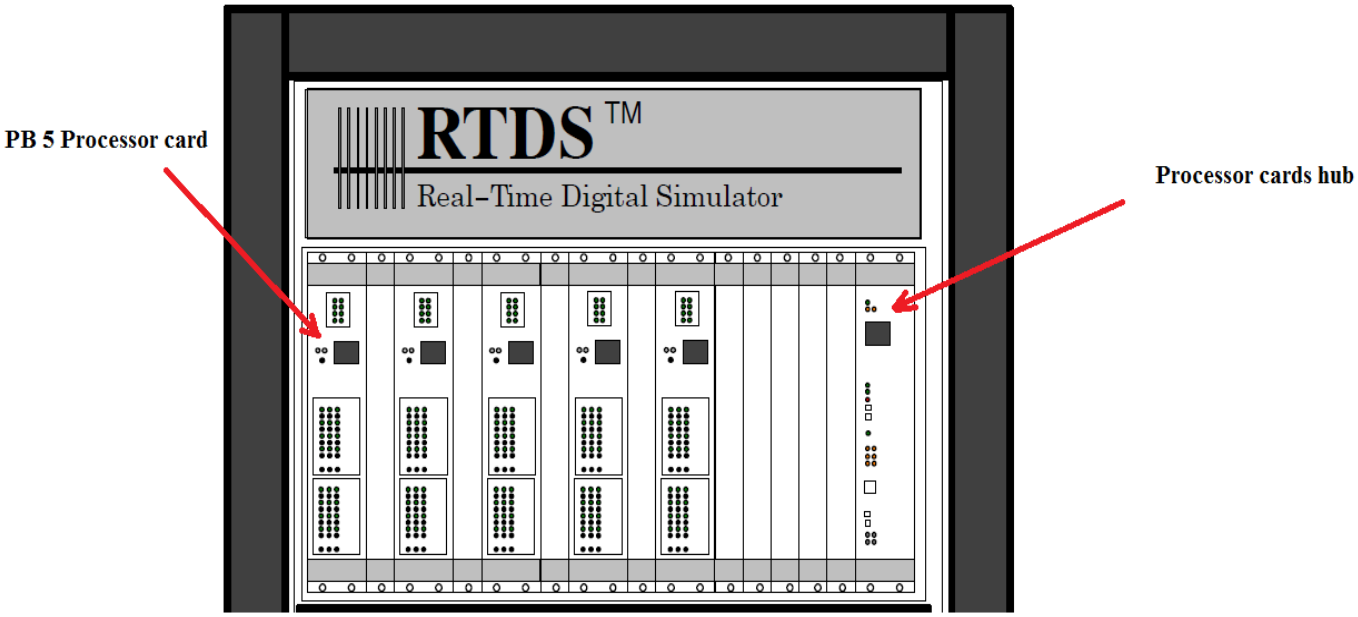

Figure 5.7 RTDS rack structure [24]

The PB5 card represented in Figure 5.7 is the processor card used to solve the equations representing the power system and control system components modelled within the RTDS and each of those network solutions can include a maximum of 90 single-phase nodes [24].

Signals from PB5 cards are sent to GTAO cards by two fibre cables and from GTAO card 12 analogical signals are created in 12 separate outputs as shown in Figure 5.8. Separate wires are used for each phase of current and voltage for connection to amplifiers.

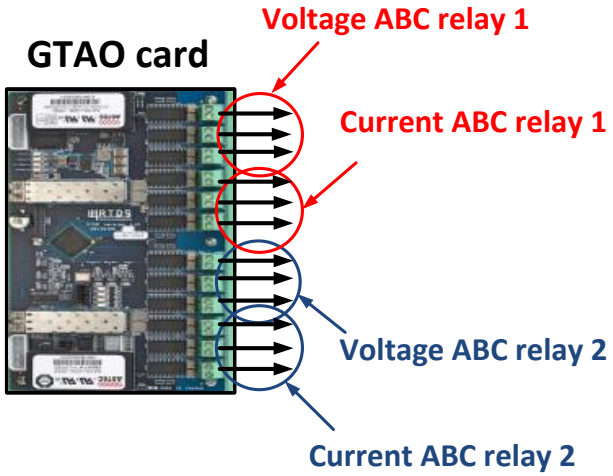

Figure 5.8 GTAO card connections

As shown in Figure 5.1 output cables of amplifiers are connected to numerical relays. Diagram indicated in appendix B explains wiring for relay connection for test setup. Analogical signals from amplifiers are interconnected with ports Q1, Q3, Q5, and Q7 for voltages and R15, R16, R17 and R18 for currents.

The binary signals for tripping breaker phases A, B, C and binary signals for autorecloser provided by the numerical relay ports K6, K7, K8 and B013 are connected to digital channels front panel shown in Figure 5.9.

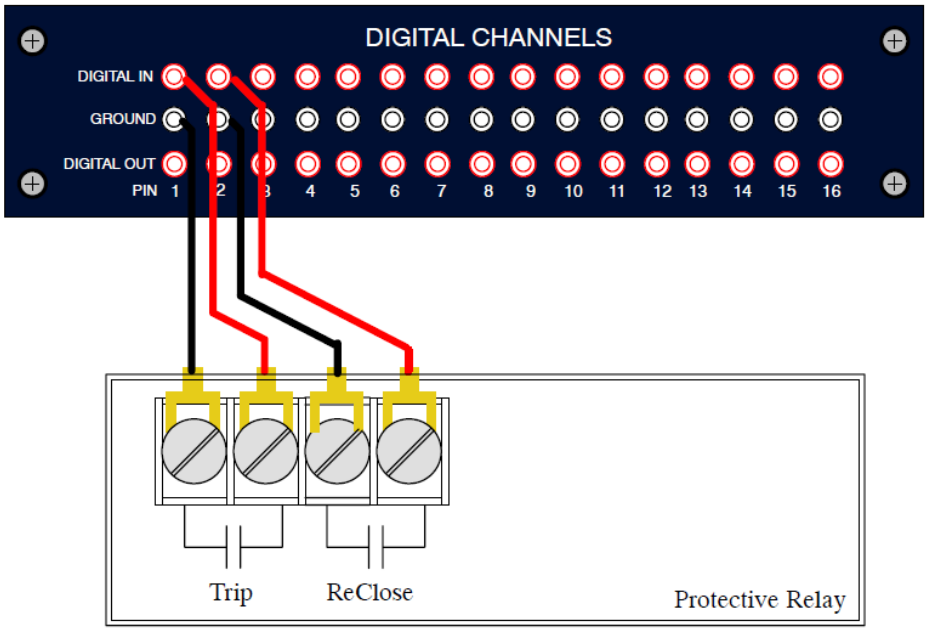

Figure 5.9 Digital Channels Front Panel structure [25]

The digital channels front panel is serving the purpose to interface up to 16 digital input signals between the RTDS and relay protection device for trip and reclose in RSCAD. A breaker modelled in RSCAD software can be made to respond to digital signals interfaced via the digital channels front panel. A relay's trip and reclose signals are typically dry contacts and the GTFPI card includes 1 kOhm pull up resistors to a 5 volt supply so dry contact operation is possible. An open connection between the Digital In and Ground results in a logic '1' being read while shorting the Digital In to Ground results GTFPI Card in a logic 0 being read [25].

Signals from digital channels front panel are forwarded to GTFPI card as shown in Figure 5.10 and connected by ribbon cable connectors to *I/O Panel Connector* point.

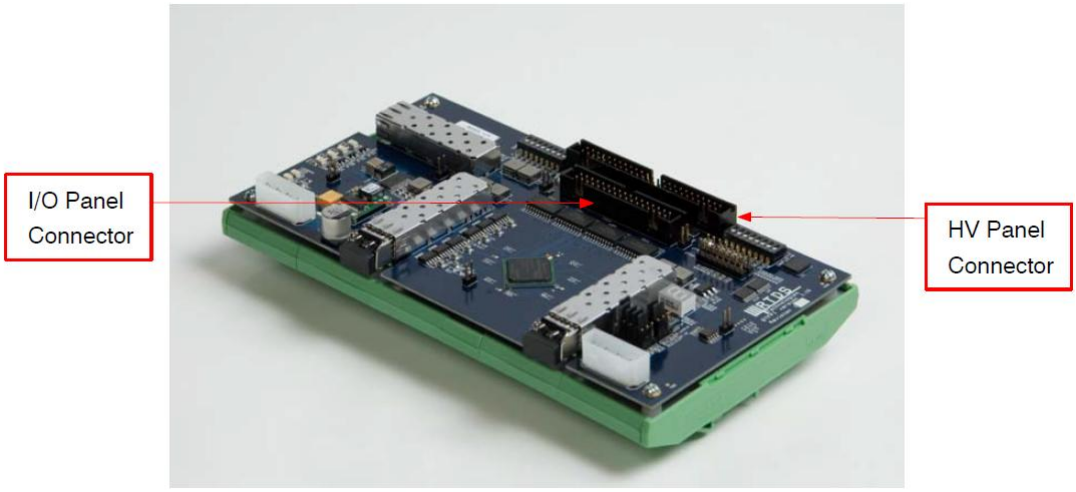

Figure 5.10 GTFPI card connections [25]

GTFPI card signals are sent back to PB 5 processor cards and via internet to virtual breakers in test system model in RSCAD software.

Figure 5.6 shows signals *40signalA, 40signalB and 40signalC* containing data about status of the virtual breaker per phase. These signals are constantly sent from GTFPI block in RSCAD to relay protective device via high voltage digital interface front panel represented in Figure 5.11. The GTFPI card acts here also as the interface card between the RTDS processor card (GPC) and the HV panel [25].

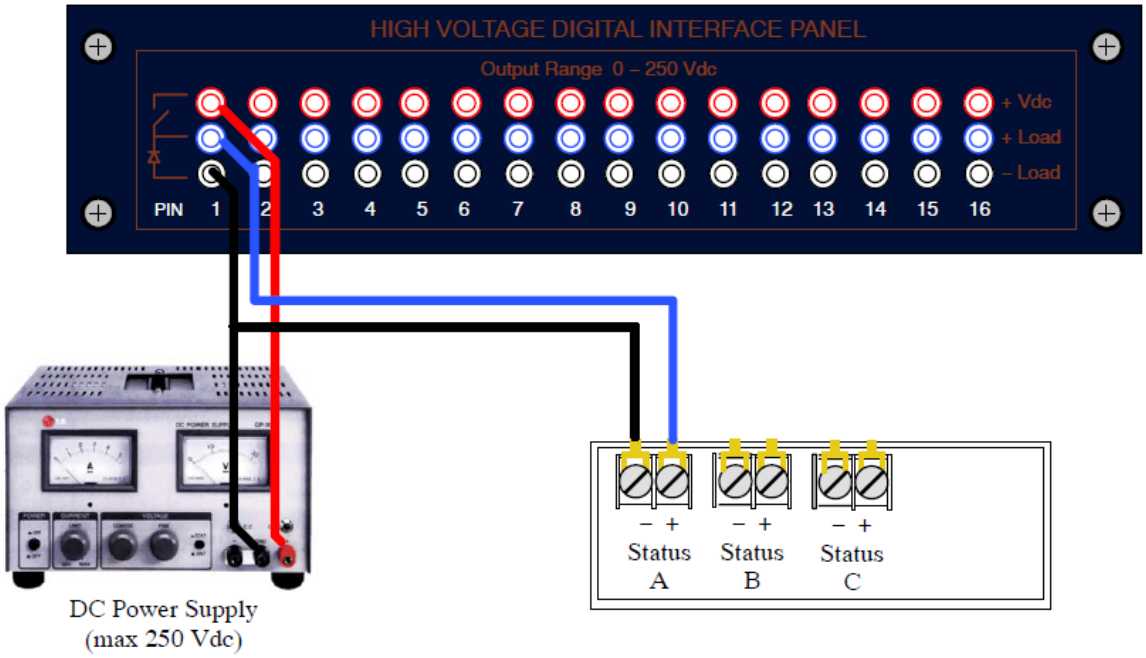

Figure 5.11 HV Panel Connection for Breaker Status Signals which require an external supply voltage [25]

The commercial relay under consideration in this test setup requires the signals with DC voltage approximately 125 V to indicate status of each phase in the virtual breaker. The high voltage digital interface front panel is able to create signals with DC voltage up to 250 V. The high voltage panel consists of solid state switches which are linked to external voltage source as shown in Figure 5.11.

Each of the 16 output channels on the high voltage interface front panel include a solid state switch between the +Vdc and +Load terminals. The solid state switches are installed in sockets on a backplane mounted to the rear of the HV Panel. A ribbon cable connects between the backplane and the GTFPI card. Signals from the GTFPI card are used to control the status (open or closed) of the solid state switches. Power for the backplane (+5Vdc) is obtained from the rack main power supply in the RTDS.[25]

Finally breaker status signals comes to the ports *J3, J4, J5 and J6* of protective relay as indicated in appendix B.

In this way the loop for testing is closed and the test of relay protection could be conducted.

5.4 Script for Testing

A script for automated calculations was created in RSCAD internal tools shown in Figure 5.12 to simulate repetitive cases and accelerate research process. The flow chart of script logic is represented in Figure 5.13 and includes 3 loops.

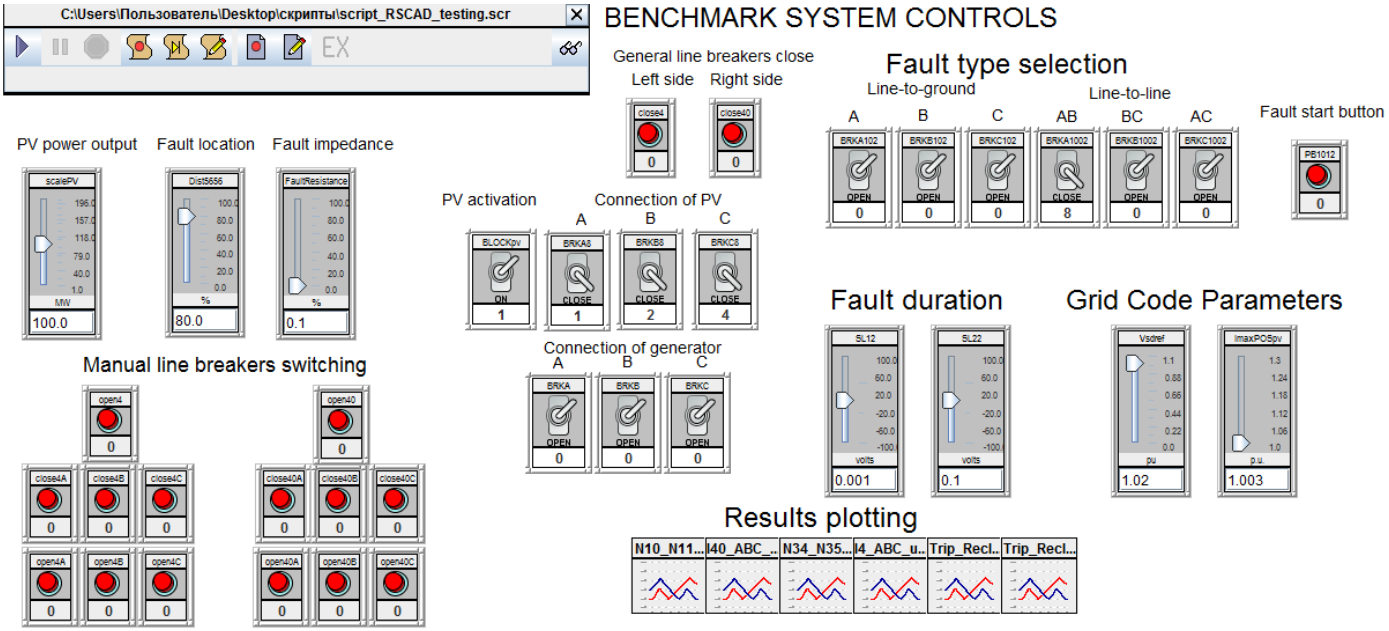

Figure 5.12 RSCAD runtime model

The first inner loop is responsible for change of fault type. Fault types includes line-to-ground, line-to-line, two lines-to-ground for all phase combinations and balanced faults.

The second loop is used for change of fault location in percentage of line distance. In this test setup the distances of 50%, 70%, 75%, 77%, 80%, 82%, 85% and 90% are considered but any other values can be added to this list.

The third outer loop is changing the fault impedance between 0.1 Ohm, 1 Ohm, 10 Ohm and 100 Ohm.

Overall 320 simulations are provided for one test scenario. This procedure is repeated three times to validate correctness of results.

For each test scenario a separate folder is created by script and all plots of currents, voltages and binary trip action signals are automatically saved in format of ".out" files. In order to accelerate results evaluation process the separate script was written in Matlab for plotting. It creates plots for each simulation in one page with proper formatting defined by user.

Both script in RSCAD for testing and script in Matlab for plotting are represented in appendix C.

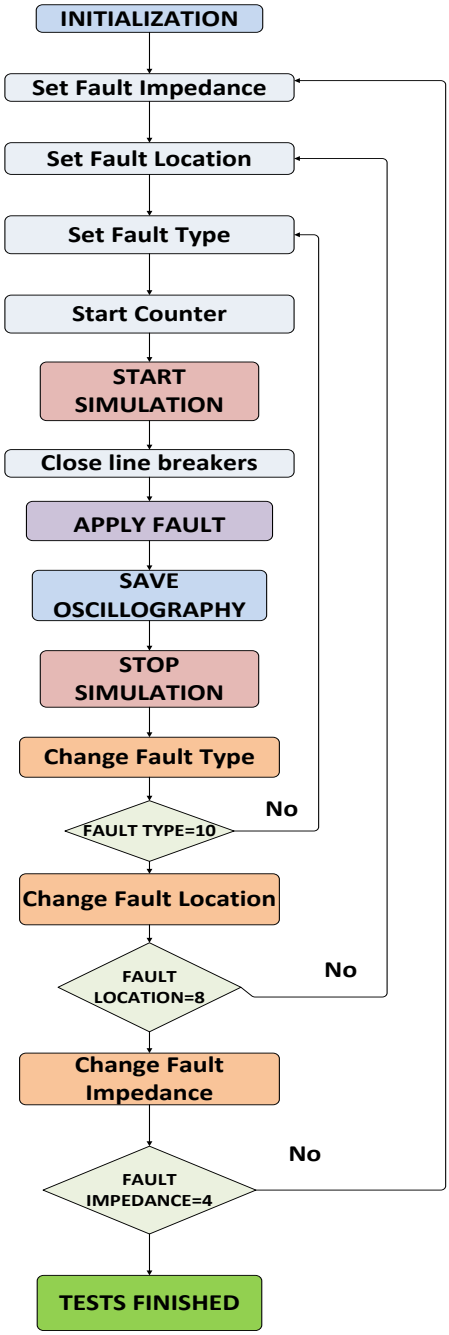

Figure 5.13 Flow chart of script for relay testing

6. Testing of Distance Protection

6.1 Introduction

Distance protection function of two relays was tested in the hardware-in-the-loop setup. The results were recorded and plotted in Matlab and in graphic interface of relay commercial software. Binary signals of tripping and reclosing actions, voltages and currents, impedance trajectories were estimated for each case.

Up to 100000 test scenarios were considered. An script for automated calculation was applied to accelerate testing process, simulating 5 cases per minute.

All cases of protective relay maloperation were identified and studied. Simulation results are represented in this chapter and explained from mathematical point of view.

6.2 Test Scenarios

The benchmark system was designed to simulate the case of gradual replacement of traditional sources by renewables. Originally, the system was fed only by synchronous generators from conventional power plant. Later PV generation was increased step by step while synchronous generator power output in the grid was declining. In order to check all critical current output and impedance reach three different test cases were considered.

1) First case considers 100MVA produced by synchronous generator

2) Second case is considering connection of both PV plant and synchronous generator with different share of generation according to Table 6.1.

Table 6.1 Generation output for different cases

Number of the case	Synchronous generators power output, MVA	Share of whole generation in %	Share of whole generation in %	PV power output, MVA
1	80 MVA	80%	20 %	20 MVA
2	60 MVA	60 %	40 %	40 MVA
3	50 MVA	50 %	50 %	50 MVA
4	40 MVA	40 %	60 %	60 MVA
5	20 MVA	20%	80 %	80 MVA

3) Third case considers contingency of the conventional power plant. 100MVA is produced by PV plant

Several points of fault occurring on the line under consideration were estimated. In order to check the selectivity of relay the fault locations close to boundary of protection zones equals to 80% of 30km line were considered.

Four types of fault were simulated: line-to-ground fault, line-to-line fault, two lines-to-ground fault and balanced three phases fault.

Also four options of fault resistance were considered: first one is bolted fault with 0.1 Ohm, the second is impedance fault with 1 Ohm, the third and the fourth are 10 Ohm and 100 Ohm correspondingly.

6.3 Simulation Results

The first test criterion was the correct operation in the event of fault appearance in different locations at the line. The line impedance in this test equals to 0.1 Ohm.

The first test scenario proved that relay located closer to generator operates correctly for all type of faults with conventional power plant connection at the end of radial line as shown in Table 6.2. Locations 50%, 70%, 75%, 77% and 80% of the line under consideration are placed in the first zone of distance protection function. The distance of 80% equals to 24 km is boundary between two zones. Locations 82%, 85% and 90% were correctly detected by protective relay in second zone in accordance with settings.

Table 6.2 Distance relay performance for different fault locations

Scenario	**Fault Location %**	**Line-to-ground**		**Line-to line**		**Two lines-to-ground**		**Balanced**	
		Zone 1	Zone 2	Zone 1	Zone 2	Zone 1	Zone 2	Zone 1	Zone 2
Conventional Power Plant	50	x	-	x	-	x	-	x	-
	70	x	-	x	-	x	-	x	-
	75	x	-	x	-	x	-	x	-
	77	x	-	x	-	x	-	x	-
	80	**x**	**-**	**x**	**-**	**x**	**-**	**x**	**-**
	82	-	x	-	x	-	x	-	x
	85	-	x	-	x	-	x	-	x
	90	-	x	-	x	-	x	-	x
Conventional Power Plant and PV Plant	50	x	-	x	-	x	-	x	-
	70	x	-	x	-	x	-	x	-
	75	x	-	x	-	x	-	x	-
	77	x	-	x	-	x	-	x	-
	80	**x**	**-**	**x**	**-**	**x**	**-**	**x**	**-**
	82	-	x	-	x	-	x	-	x
	85	-	x	-	x	-	x	-	x
	90	-	x	-	x	-	x	-	x
PV Plant	50	x	-	-	-	x	-	-	-
	70	x	-	-	-	x	-	-	-
	75	x	-	-	-	x	-	-	-
	77	x	-	-	-	x	-	-	-
	80	**x**	**-**	**-**	**-**	**x**	**-**	**-**	**-**
	82	-	x	-	-	x	-	-	-
	85	-	x	-	-	-	x	-	-
	90	-	x	-	-	-	x	-	-

The second test scenario with different share of conventional and PV generation demonstrated that the behavior of relay is the same as during the first test scenario when only synchronous generator was connected. It can be explained by two parameters of generator which play important role during transient process *Xd* and *Xd*' indicated in Table 4.2 previously. *Xd* is also called synchronous reactance which represent generator impedance during steady-state while *Xd*' is transient reactance defining generator during fault conditions. The ratio of *Xd*'/*Xd* equals to approximately 6. It means that current injection of synchronous generator will increase exponentially during fault state. Generator current injection will be dominant even if PV plant capacity will be equal to 80% of whole generation because the value of reactance *Xd* and *Xd*' are not changing.

The third test scenario with only PV plant connection revealed that distance protection function failed to operate during line-to-line and balanced faults at any fault location. These types of faults are not involving ground for impedance calculations and zero sequence components equal to zero. Moreover the positive and negative injected currents are limited by power electronic inverter which leads to maloperation of protective relay.

Also for two lines-to-ground fault at the location 82% of the line the relay tripped in the first zone. This fact indicated the degradation of protection selectivity and can cause tripping without delay during fault placed at the other element in the system.

The second test criterion was the correct operation in case of different fault impedances. The fault location during this test was equal to the 80% of the line or 24 km. For correct operation the relay should trigger in the first zone as in previous test. The results of this test are represented in Table 6.3.

Table 6.3 Distance relay performance for different fault impedances

Scenario	Fault impedance(Ohm)	Line-to-ground		Line-to line		Two lines-to-ground		Balanced	
		Zone 1	Zone 2	Zone 1	Zone 2	Zone 1	Zone 2	Zone 1	Zone 2
Conventional Power Plant	0.1	x	-	x	-	x	-	x	-
	1	x	-	x	-	x	-	x	-
	10	x	-	-	-	-	-	-	-
	100	-	-	-	-	-	-	-	-
PV Plant	0.1	x	-	-	-	x	-	-	-
	1	x	-	-	-	x	-	-	-
	10	x	-	-	-	-	-	-	-
	100	-	-	-	-	-	-	-	-

The first test scenario showed that distance protection function is able to detect the fault with impedances up to 1 Ohm for any type of fault and even up to 10 for line-to-ground fault when conventional power plant is connected.

The second test scenario revealed that protective relay operates correctly if fault impedance equals up to 10 Ohm for line-to-ground faults and up to 1 Ohm for two lines-to-ground faults. In other cases relay maloperate and is not able to identify the fault.

Explanation of processes which took place and cause maloperation of the distance protection function during each type of fault is considered in details below.

6.3.1 Line-to-ground Fault

The line-to-ground fault is typically detected in both test scenarios. As represented in Figure 6.1 the current injection during transient conditions when synchronous generator is connected is very high and relay with distance protection function can easily pick up the fault. For relay placed in vicinity of the main grid the level of current injection is much higher because it is determined by the system strength or impedance of the system.

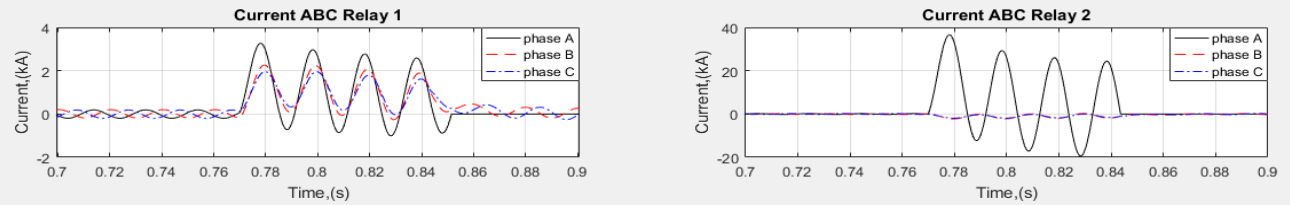

Figure 6.1 Fault current in relays during line-to-ground fault with conventional generation

Time of trip action is shown in Figure 6.2. It is less than 150 ms as required in [16]. The black colour means that only phase A was tripped by relay and after one second it was reclosed. For both relays during generator connection the tripping signals are correct and appeared in right time.

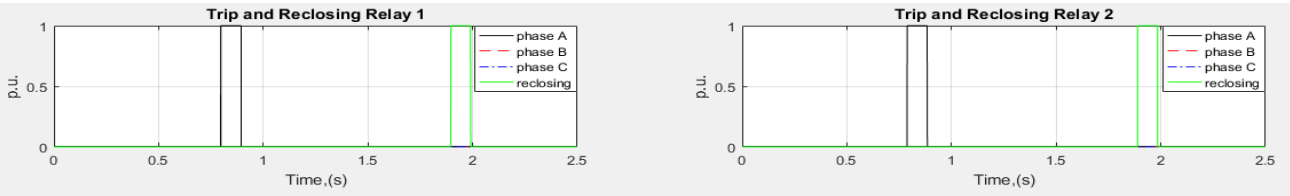

Figure 6.2 Trip and reclosing signals during line-to-ground fault with conventional generation

Impedance reaches for different fault impedance values are indicated in Figure 6.3. Due to the fact that line-to-ground element for detection is used the impedance trajectories are plotted in the quadrilateral characteristics. At least three dots are required for identification of the fault in the zone. In this case the relay operated accurate in zone 1 for 0.1 Ohm, 1 Oh, and 10 Ohm.

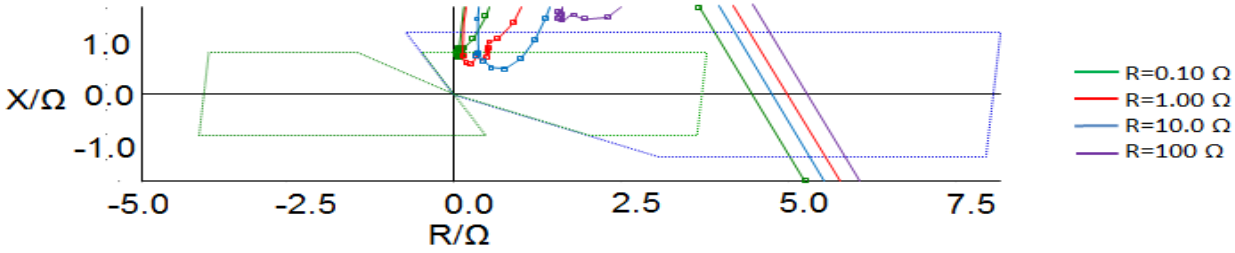

Figure 6.3 Impedance trajectories during line-to-ground fault with conventional generation

In case of PV plant connection and line-to-ground fault the current injection from PV source is sufficient for relay to pick up the fault. It happens because the zero sequence current prevailing in this type of fault and is not impacted by the control system but defined by parameters of system elements and grounding while positive and negative sequence currents are limited by inverter control to approximately 1.2 p.u.

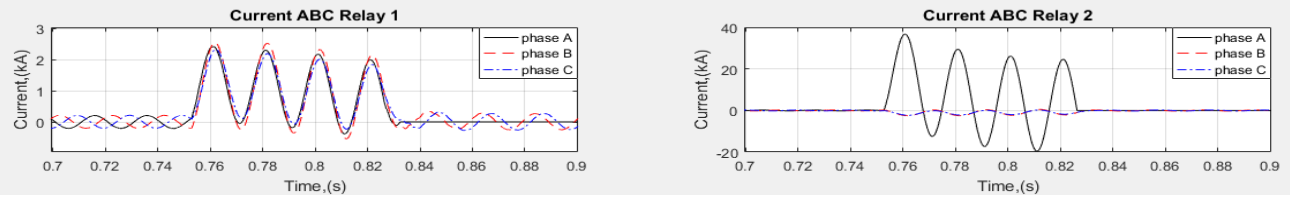

Figure 6.4 Fault current in relays during line-to-ground fault with PV generation

Thus both relays triggered properly at 0.77 seconds and sent reclosing signal at 1.77 seconds as shown in Figure 6.5.

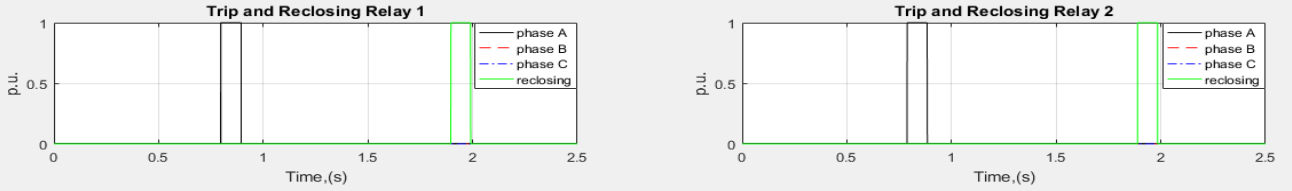

Figure 6.5 Trip and reclosing signals during line-to-ground fault with PV generation

Impedance trajectories are more distorted during PV connection compared to conventional power plant as indicated in Figure 6.6. The blue line 10 Ohm trajectory is nearly failed to reach the correct zone. But as in the previous case the distance protection function still detects faults with impedances up to 10 Ohm for line-to-ground faults.

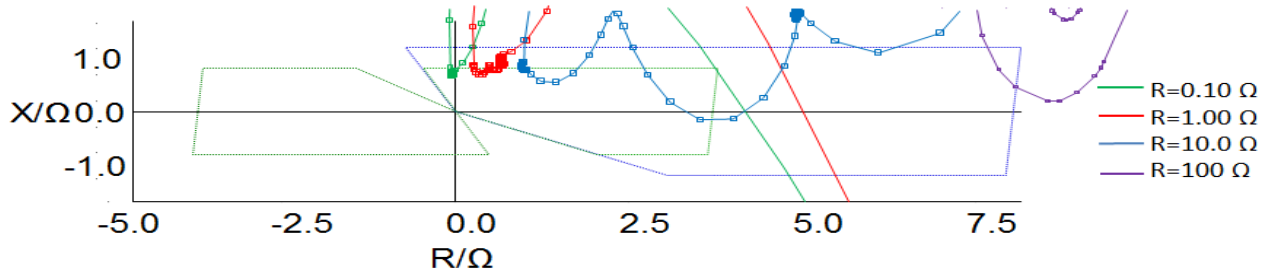

Figure 6.6 Impedance trajectories during line-to-ground fault with PV generation

In such a way the line-to-ground faults are not creating any critical issues for relay with distance protection function operation.

6.3.2 Line-to-line Fault

The line-to-line fault is nicely detected during generator connection. As shown in Figure 6.7 the current injection of phases A and B is several times bigger than load current during transient conditions for the first relay. The distance protection can easily pick up the fault. For the second relay shown in the right plot the situation is the same.

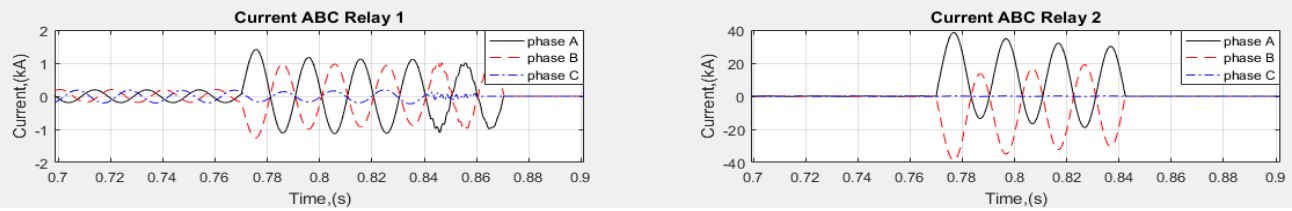

Figure 6.7 Fault current in relays during line-to-line fault with conventional generation

Trip and reclosing signals from relay with distance protection function were sent correctly as represented in Figure 6.8. Three phases of breaker were tripped and reclosed after line-to-line fault detection.

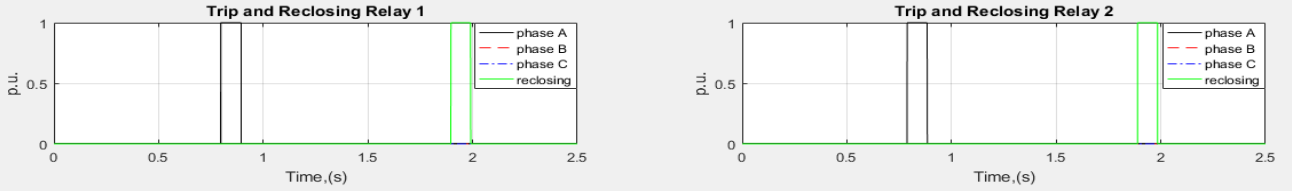

Figure 6.8 Trip and reclosing signals during line-to-line fault with conventional generation

For line-to-line faults the Mho characteristic is used to check correctness of impedance trajectories shown in Figure 6.9. The impedance reach for faults with impedances 0.1 Ohm and 1 Ohm is coming to correct zone while fault impedance of 10 Ohm is far to the right from any zone. It can be explained by extra fault resistance which must be added to the impedance calculated by distance relay. It force trajectory to move to the right. The trajectory of impedance fault 100 Ohm is not visible because it is too far to the right.

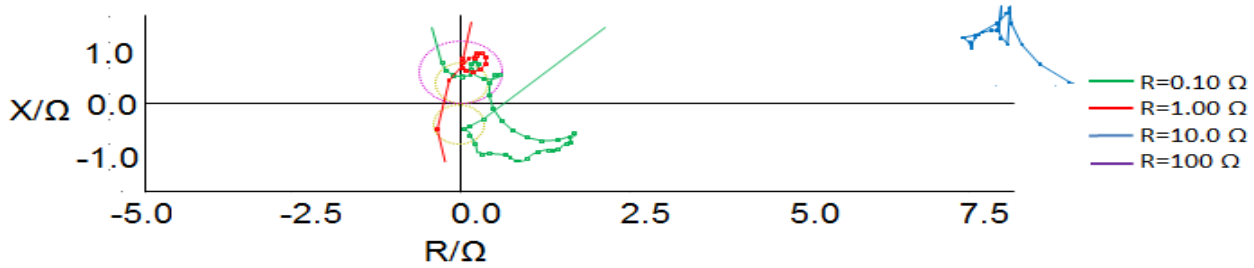

Figure 6.9 Impedance trajectories during line-to-line fault with conventional generation

Based on Figure 6.10 in case of PV plant connection and line-to-line fault the injected fault current is close to load current and relay can't pick fault up. Meanwhile in the second relay the fault detection is perfectly done due to high current values.

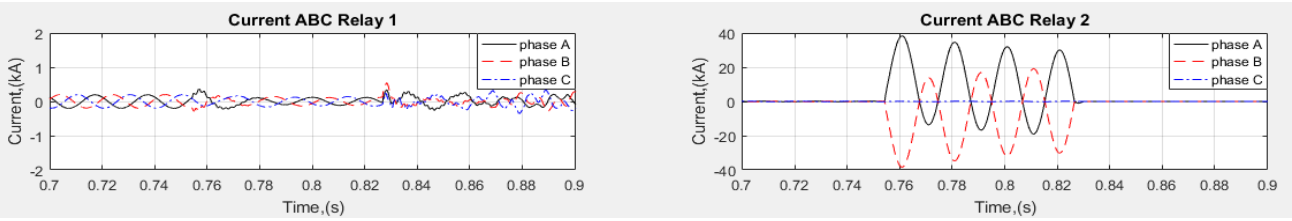

Figure 6.10 Fault current in relays during line-to-line fault with PV generation

Therefore, the first relay didn't supply any signals to breaker while the second relay sent them properly according to Figure 6.11.

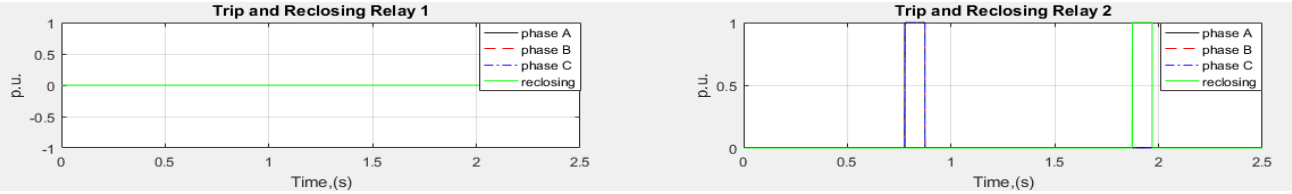

Figure 6.11 Trip and reclosing signals during line-to-line fault with PV generation

What is more, the only impedance fault with R=0.1 Ohm had trajectory coming to proper zone shown green in Figure 6.12. The rest impedance reach lines indicated in red and blue are shifter to the right side far from Mho characteristics.

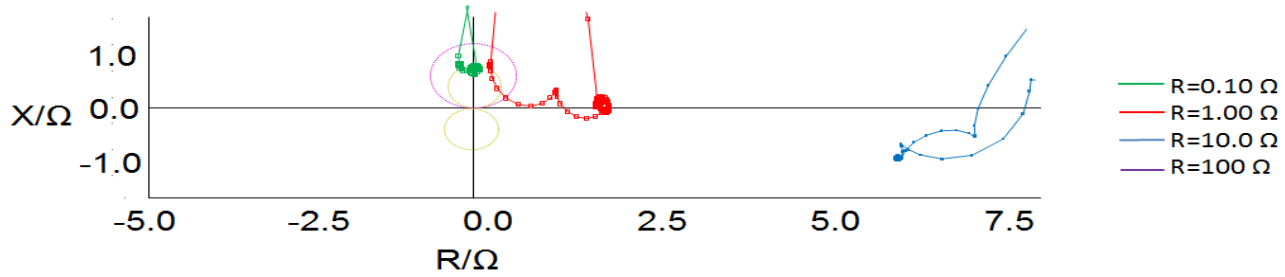

Figure 6.12 Impedance trajectories during line-to-line fault with PV generation

Thus, the maloperation of distance protection function during the line-to-line fault is caused by low current injection mainly and additionally is worsen by wrong impedance trajectories calculation.

6.3.3 Two Lines-to-ground Fault

As in case of the line-to-ground fault, two lines-to-ground fault didn't face current injection problems because of dominant zero sequence current component. The fault currents of both relays during connection of synchronous generator are represented in Figure 6.13.

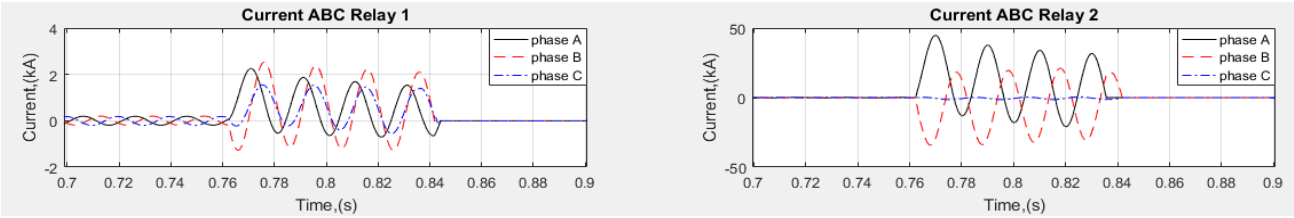

Figure 6.13 Fault current in relays during two lines-to-ground fault with conventional generation

That is why the protective relays triggered properly and had trip and reclosing binary signals shown in Figure 6.14.

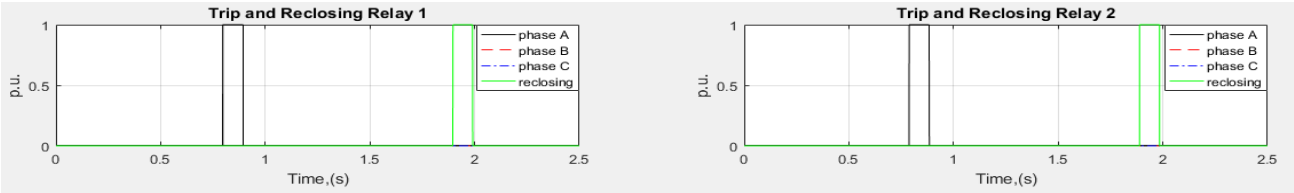

Figure 6.14 Trip and reclosing signals during two lines-to-ground fault with conventional generation

In order to detect the two lines-to-ground fault two impedance characteristics are presented in Figure 6.15. Only faults with impedance up to 1 Ohm were calculated correctly. The higher values of impedance faults are not visible in scale of this plot.

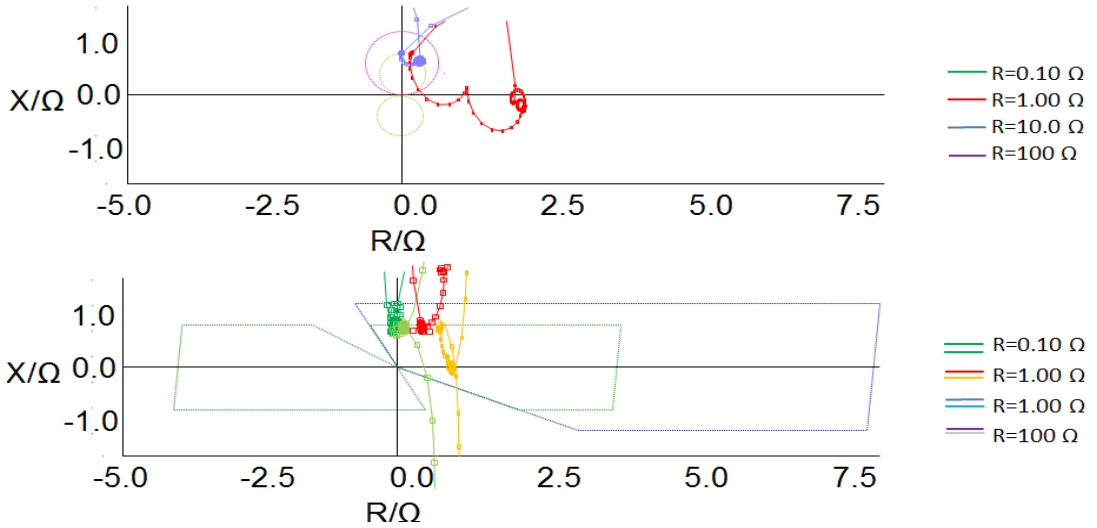

Figure 6.15 Impedance trajectories during two lines-to-ground fault with conventional generation

All three phases increased the current values when PV plant was connected in the first relay. Zero sequence currents and lack of positive sequence current component created such wave shape. The second relay can be considered as a reference how relay operates in perfect case.

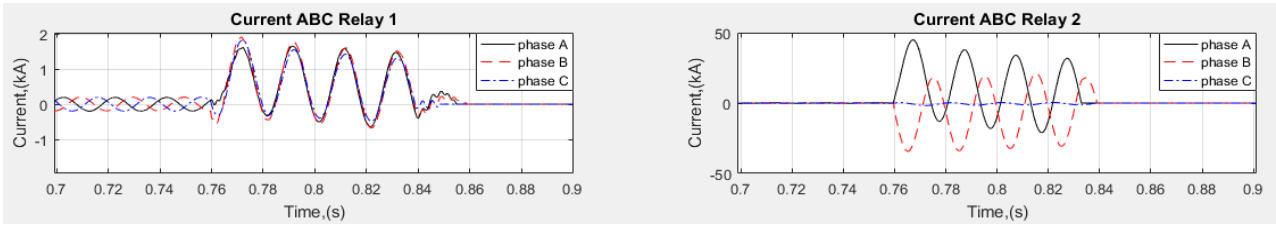

Figure 6.16 Fault current in relays during two lines-to-ground fault with PV generation

Three phase binary tripping signals and reclosing after 1 second during the two lines-to-ground faults are correctly generated by the first and the second relays as shown in Figure 6.17.

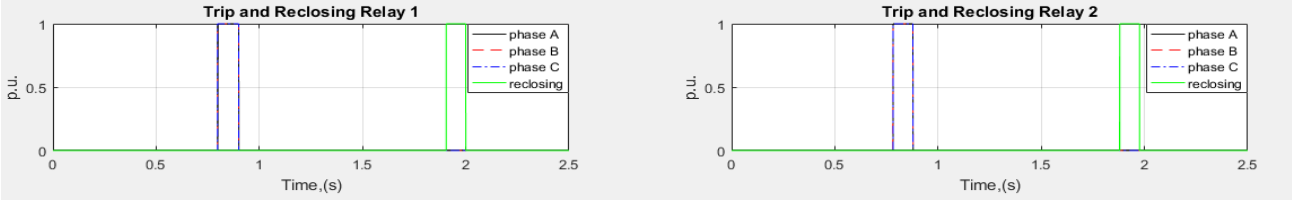

Figure 6.17 Trip and reclosing signals during two lines-to-ground fault with PV generation

Impedance reaches of 0.1 Ohm and 1 Ohm during the two lines-to-ground faults and PV connection are presented in Figure 6.18. The trajectories are more distorted than during synchronous generator connection because of intermittent nature of PV plant. The impedance faults higher than 1 Ohm are not visible in Figure 6.18 and placed in the right side of the plot.

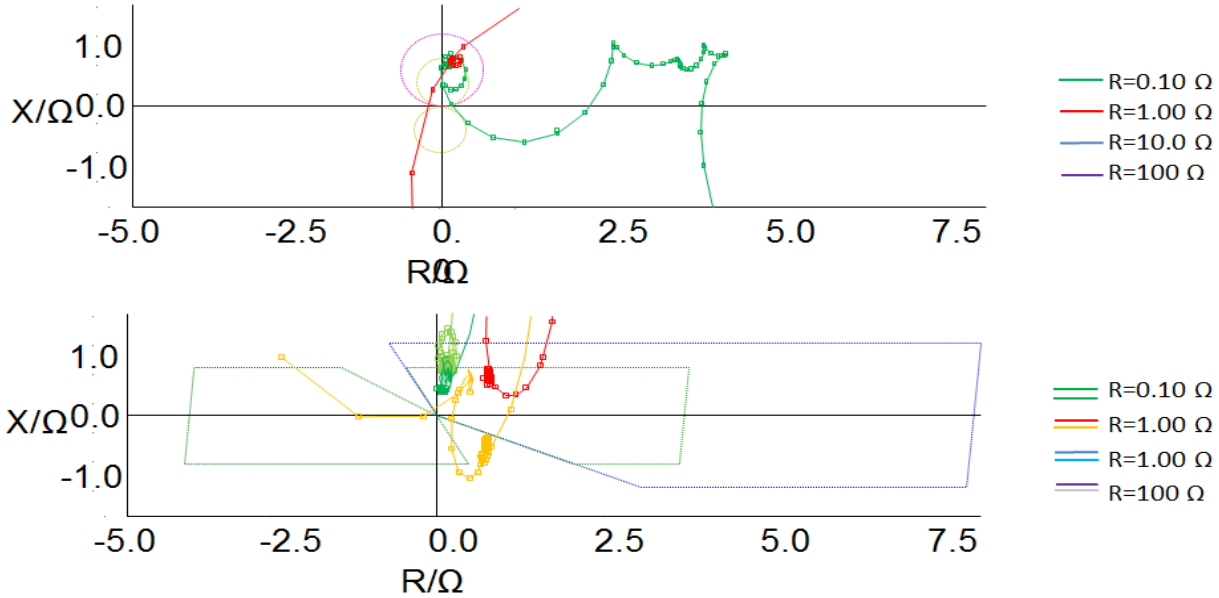

Figure 6.18 Impedance trajectories during two lines-to-ground fault with PV generation

Therethrough the two lines-to-ground faults are not causing serious problems for proper distance protection operation.

6.3.4 Balanced Fault

Three phase or balanced faults are not involving zero sequence or negative sequence and consists only from positive sequence which is controlled by inverter logic in case of PV connection and generator controls in case of conventional power plant connection. The fault injection current shown in Figure 6.19 is twice more than load current for the first relay and protective relay is easily pick the fault up.

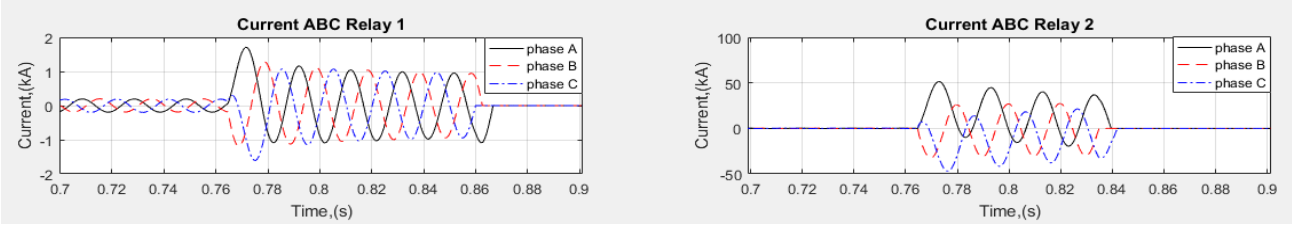

Figure 6.19 Fault current in relays during balanced fault with conventional generation

As a result of nice current injection the relay sent correct tripping signals and reclosing commands to the breaker according to Figure 6.20.

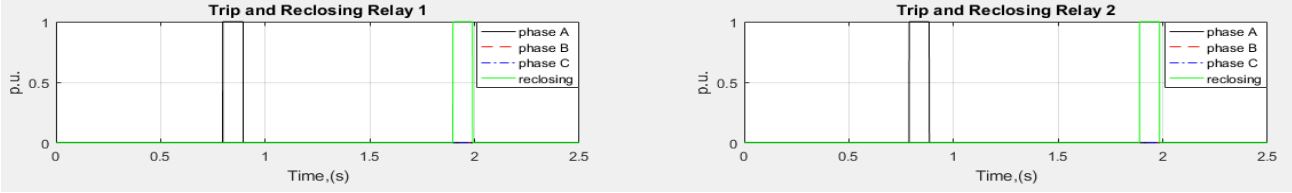

Figure 6.20 Trip and reclosing signals during balanced fault with conventional generation

Impedance trajectories are shown only for R=0.1 to avoid confusion of lines on the plot. For resistances up to 1 Ohm it operates correctly while for 10 Ohm and 100 Ohm the impedance reach is far from characteristic zones.

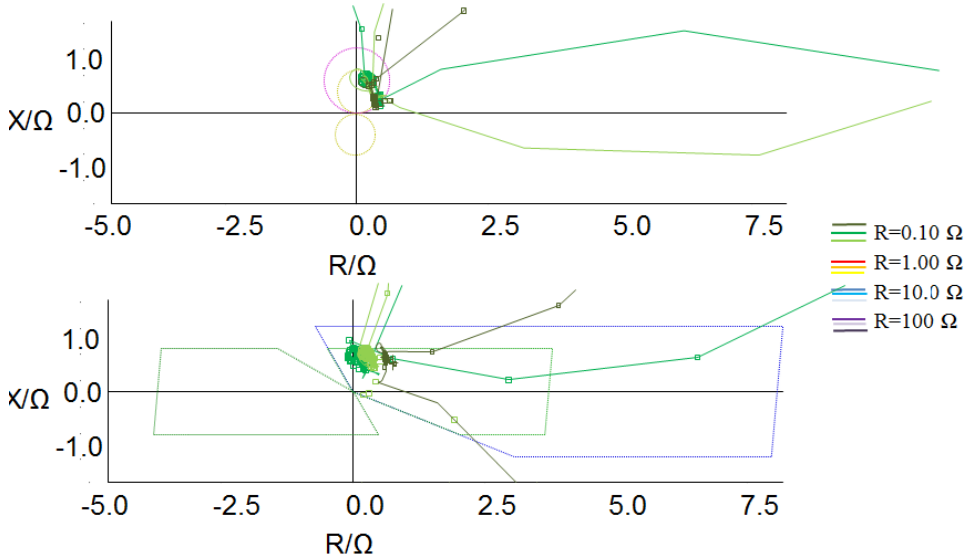

Figure 6.21 Impedance trajectories during balanced fault with conventional generation

In case of PV plant connection the positive sequence current is limited by inverter capability and logic. That is why the injection current in the first relay in Figure 6.22 is very small compared to the second relay. It causes failure in distance protection function operation because the relay didn't pick up the fault based on current level.

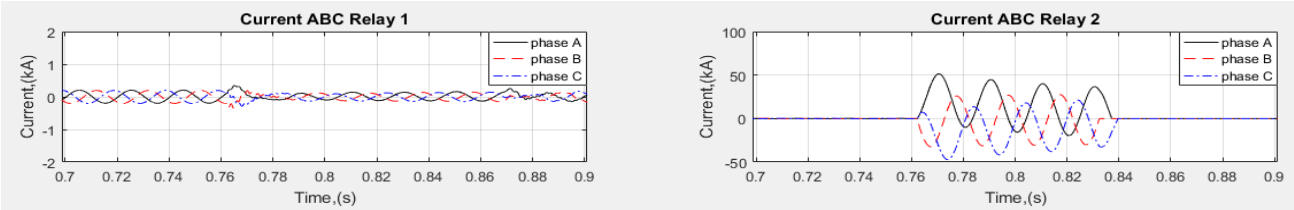

Figure 6.22 Fault current in relays during balanced fault with PV generation

As a result the binary signals for tripping in Figure 6.23 are not created by the first relay while the second one is operating correctly.

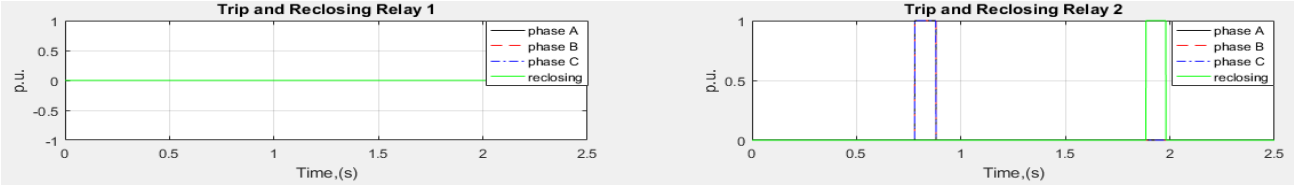

Figure 6.23 Trip and reclosing signals during balanced fault with PV generation

The impedance trajectories represented in Figure 6.24 shows the impedance fault reach with R=0.1 Ohm. The deviations of trajectory are quite serious but in the end they come to correct zone.

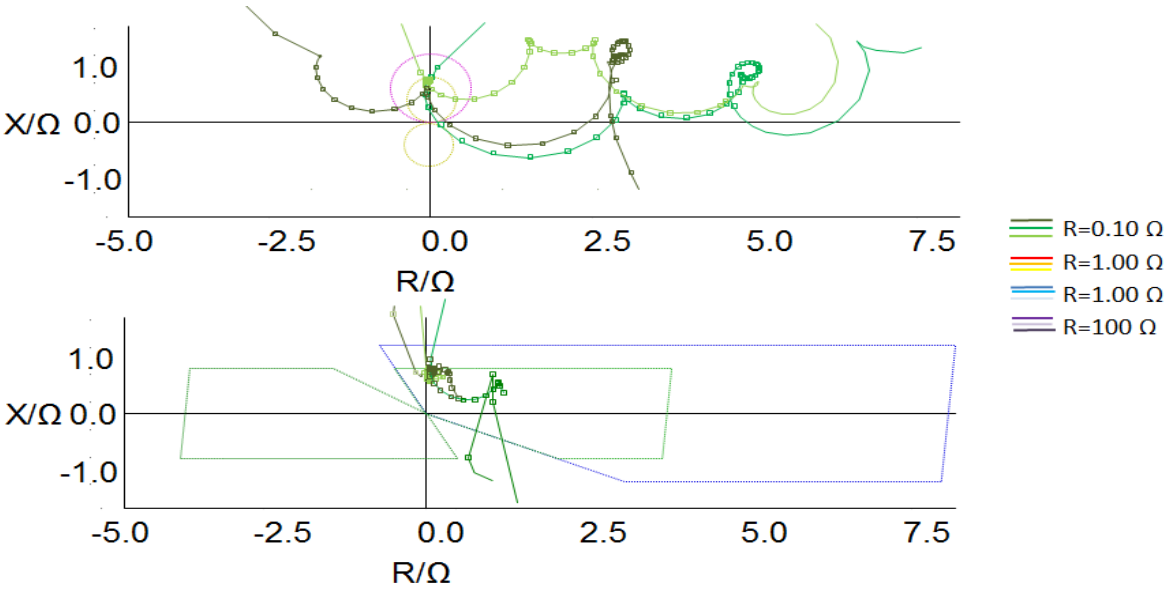

Figure 6.24 Impedance trajectories during balanced fault with PV generation

Therefore the conclusion about balanced three phase fault can be made that the main problem for detection of this type of fault is in low current injection which makes impossible to pick up the relay. The impedance reach is calculated correctly for this case.

7. Conclusion and recommendations

7.1 Conclusion

A hardware-in-the-loop test setup including benchmark model had been created with RTDS real-time simulator and commercial relays. In the RSCAD platform, the benchmark model including the control logic of the PV had been developed. The hardware-in-the-loop setup can test the performance of actual relays under different grid scenarios. The benchmark is accomplished with a script which can simulate up to 300 cases in 1 hour switching from one to another condition without the necessity of human operation.

Summarizing all extreme cases of low fault current occurrence and deviated impedance trajectories it is evident that PV plant which is fully interconnected with grid via DC-AC power electronic converter and placed in the end of radial line can create a danger for distance protection if there are no synchronous generators connected to the same bus. Even one synchronous generator connected to the same bus will provide sufficient current injection during fault state.

The line-to-line faults and balanced faults can cause maloperation of the relay in case of PV plant connection due to high dependence from positive sequence current controlled and limited by inverter.

During 100% penetration of PV sources the impedance reach started to deviate from common trajectory but still came to correct zone. It can create the problems for distance protection if several factors will coincide like high PV power output and high impedance fault.

Due to the fast control used in the PV system, there were no problems with delay, underreach or overreach cases. Nevertheless, this cases can appear when another type of renewable generator is connected to the system (i.e. wind turbines systems).

The detection of line-to-ground fault and two lines-to-ground faults by distance protection is not affected by the type of source: conventional power plant or PV plant.

As a result of the research the conclusion is made that PV plants placed in the end of radial line can create a danger for distance protection.

7.2 Recommendations

The set of recommendations to manage the challenge shown in benchmark system was suggested:

1. PV plants should be placed in the vicinity of conventional power plants if terrain allows it.
2. The distance relay current setting must consider possible outage of traditional power plant (n-1 criteria).
3. Differential relay protection is less vulnerable to low fault current and can be used instead of distance protection.
4. Week infeed function and echo signal for teleprotection can improve sensitivity of distance protection.

7.3 Further Research

The further research statements were formulated for continuation of the research

1. The controls of grid inverter and grid codes can be enhanced to allow larger current injection during fault occurrence

2. Logic of distance relay can be revised to enable detection of fault during low current conditions

Bibliography

[1]. European Commission (EU) (2018). *2030 climate & energy framework* [Online]. Available: https://ec.europa.eu/clima/policies/strategies/2030_en

[2]. The White House (US) (2016). *North American Climate, Clean Energy, and Environment Partnership Action Plan* [Online]. Available: https://obamawhitehouse.archives.gov/the-press-office/2016/06/29/north-american-climate-clean-energy-and-environment-partnership-action

[3]. Australian Government (AU) (2015). *Australia's 2030 Emissions Reduction Target* [Online]. Available: http://www.environment.gov.au/system/files/resources/f8f337c2-2d58-4d70-a1fd-acc71254a137/files/factsheet-2030-emissions-reduction-target.pdf

[4]. W. Schossig (2008). *Distance Protection: The Early Developments Distance Protection (Distanzschutz. Der Beginn und die ersten Schritte*) [Online]. Available: http://www.pacw.org/fileadmin/doc/WinterIssue08/history_winter08.pdf

[5]. W. Schossig (2008). *History Distance Protection – From Protection Relays to Multifunktional (Die Schritte des Distanzschutzes zum multifunktionalen Abzweigschutz* [Online]. Available: http://www.pacw.org/fileadmin/doc/SpringIssue08/history_spring08.pdf

[6]. Anderson, P.M. (1999). *Power System Protection*. Hoboken: John Wiley & Sons.

[7]. T.Neumann, I. Erlich (2012). *Short Circuit Current Contribution of a Photovoltaic Plant*. The 8th Power Plant and Power System Control Symposium, France, FR, pp. 343-348.

[8]. M.Mirhosseini, J. Pou, B.Karanayil, V.Agelidis (2013). *Positive-and Negative-Sequence Control of Grid-Connected Photovoltaic Systems under Unbalanced Voltage Conditions*. Australasian Universities Power Engineering Conference, Tasmania, TAS, pp.345-361.

[9]. A.Hooshyar, M. Azzouz,E.El-Saadany (2015). *Distance Protection of Lines Emanating From Full-Scale Converter-Interfaced Renewable Energy Power Plants – Part I: Problem Statement*. IEEE transactions on power delivery, France, FR, pp.1770-1780.

[10]. A.Hooshyar, M. Azzouz,E.El-Saadany (2015). *Distance Protection of Lines Emanating From Full-Scale Converter-Interfaced Renewable Energy Power Plants – Part II: Solution Description and Evaluation*. IEEE transactions on power delivery, France, FR, pp.1781-1791.

[11]. M. M. Alam, H. Leite, Nuno Silva, A. D. S. Carvalho (2017). *Performance evaluation of distance protection of transmission lines connected with VSCHVDC system using closed-loop test in RTDS*. Electric Power Systems, vol. 152, pp. 168-183.

[12]. J. Jia, G. Yang, A. Nielsen, P. Roenne-Hansen (2018). *Hardware-in-the-loop Tests on Distant Protection Considering VSC Fault-ride-through Control Strategies*. The 14th International Conference on Developments in Power System Protection, United Kingdom, UK.

[13]. M. Nagpal, C. Henville (2018). *Impact of Power Electronic Sources on Transmission Line Ground Fault Protection*. IEEE Transactions on Power Delivery, pp.62-70

[14]. Siemens (2016). *SIPROTEC 4 Line Differential Protection with Distance Protection 7SD5* [Online]. Available: https://w3.siemens.com/smartgrid/global/en/products-systems-solutions/protection/combined-line-differential-and-distance-protection/pages/7sd52_53.aspx

[15]. IEC *60255-121*std. (2014). *Functional Requirements for Distance Protection.*

[16]. Tennet (GE) (2015). *Onshore Grid Code* [Online]. Available: https://www.tennet.eu/fileadmin/user_upload/The_Electricity_Market/German_Market/Grid_customers/tennet-NAR2015eng.pdf

[17]. RTDS technologies (2015). *Real time digital simulation for the power industry manual set. PV array model.*

[18]. A. Smets et al (2016). *Solar energy. The physics and engineering of photovoltaic conversion technologies and systems.* Cambridge:UIT Cambridge.

[19]. G.Farivar, B.Asaei, S.Mehrnami (2013). *An Analytical Solution for Tracking Photovoltaic Module MPP*. IEEE Journal of Photovoltaics, vol.3, no.3.

[20]. R. Teodorescu, M. Liserre and P. Rodrguez (2011). *Grid converters for photovoltaic and wind power systems*. Chichester, UK: John Wiley & Sons, Ltd.

[21]. M. Ndreko, M. Popov, A.A. van der Meer, M.A.M.M. van der Meijden (2016). *The effect of the offshore VSC-HVDC connected wind power plants on the unbalanced faulted behavior of AC transmission systems*. 2016 IEEE International EnergyConference (ENERGYCON) 1–6.

[22]. P. Kundur, N. Balu, M. Lauby (2009). *Power system stability and control*. New York: McGraw-Hill.

[23]. RTDS technologies (2013). *Real time digital simulation for the power industry manual set. Electric machine models.*

[24]. RTDS technologies (2015). *RTDS Hardware manual. PB5 Processor Card.*

[25]. RTDS technologies (2017). *RTDS Hardware manual. GTFPI Front Panel Interface Card.*

Appendix

A. CMS-156 and CMS-356 amplifiers datasheet

Technical Data[2]

Voltage amplifiers		
Setting range	3-phase AC (L-N)	3 x 0 ... 250 V
	1-phase AC (L-L)	1 x 0 ... 500 V
	DC (L-N)	3 x 0 ... ±250 V
Power	3-phase AC (L-N)	3 x 75 VA at 75 ... 250 V
	1-phase AC (L-N)	1 x 150 VA at 75 ... 250 V
	1-phase AC (L-L)	1 x 150 VA at 150 ... 500 V
	DC(L-N)	1 x 212 W at ±(150 ... 250 V)
	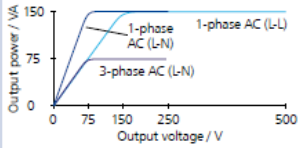	
Accuracy		error < 0.03 % typ., < 0.1 % guar.
Distortion (THD+N)[3]		< 0.03 % typ., < 0.1 % guar.
Bandwidth (-3dB)		> 6 kHz
Phase lag at 50/60 Hz[4]		1.95°/2.34°
Input voltage[5]		0 ... 5 V_{RMS}
Amplification		50 V / V
Current amplifiers		
Setting range	3-phase AC (L-N)	3 x 0 ... 25 A
	1-phase AC (L-N)	1 x 0 ... 75 A
	DC (L-N)	1 x 0 ... ±25 A
Power	3-phase AC (L-N)	3 x 70 VA at 7.5 A
	1-phase AC (3L-N)	1 x 210 VA at 22.5 A
	1-phase AC (L-L)	1 x 140 VA at 7.5 A
	DC (L-N)	1 x 140 W at ±10.5 A
	3 phase operation 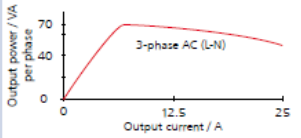	
	single phase operation 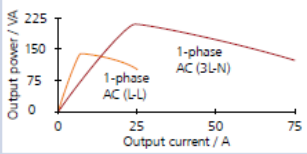	

Current amplifiers (cont.)		
Accuracy		error < 0.03 % typ., < 0.1 % guar.
Distortion (THD+N)[3]		< 0.1 % typ., < 0.3 % guar.
Bandwidth (-3dB)		> 6 kHz
Phase lag at 50/60 Hz[4]		1.88°/2.26°
Input voltage[5]		0 ... 5 V_{RMS}
Amplification		5 A / V
Max. compliance voltage (L-N)/(L-L)		15 Vpk / 30 Vpk
Amplifiers, general[6]		
Input impedance		> 40 kΩ
Galvanic isolation Input/Output		1.5 kVDC
Galvanic isolation amplifier groups		1.5 kVDC
Connection		4 mm (0.16 in) banana sockets/comb. socket
Amplifiers, if controlled by a CMC		
Frequency	range sine signals	10 ... 1000 Hz
	range transient signals	DC ... 3.1 kHz
	accuracy/-drift	±0.5 ppm / ±1 ppm
	resolution	5 µHz
Phase	angle range	- 360° ... +360°
	resolution	0.001°
	error at 50/60 Hz	< 0.02° typ., < 0.1° guar.
Output voltage resolution		12 mV
Output current resolution		1 mA
Power supply		
Nominal / permissible input voltage		110 – 240 VAC / 99 ... 264 VAC (50/60 Hz)
Permissible frequency range		45 ... 65 Hz
Power consumption		< 1000 VA
Connection		Standard AC socket (IEC 60320)
Environmental conditions		
Operation temperature		0 ... +50 °C (+32 ... +122 °F)
Storage temperature		-25 ... +70 °C (-13 ... +158 °F)
Humidity range		Relative humidity 5 ... 95 %, non-condensing
Vibration		IEC 60068-2-6 (20 m/s² at 10 ... 150 Hz)
Shock		IEC 60068-2-27 (15 g/11ms half-sine)
EMC		Directive 2004/108/EC (CE conform)
Emission		EN 61326-1, EN 61000-6-4, EN 61000-3-2/3 FCC Subpart B of Part 15 Class A
Immunity		EN 61326-1, EN 61000-6-2, EN 61000-4-2/3/4/5/6/11
Safety		Directive 2006/95/EC (CE conform) EN 61010-1, EN 60950-1, UL 61010-1, CAN/CSA-C22.2 No 61010-1-04
Miscellaneous		
Weight		14.7 kg (32.4 lbs)
Dimensions (W x H x D, without handle)		450 x 145 x 390 mm (17.7 x 5.7 x 15.4 in)
Certifications		TÜV-GS

Figure A.1 Technical data of CMS-156

Amplifiers general	
Bandwidth (-3dB)[1]	> 1 kHz
Input – Output propagation delay	500 µs (error: < ±2 µs typ., ±5 µs guar.)
Amplification at 5 Vrms input range	Voltage output: 60 V/V Current output: 6.4 A/V
Phase error at 50/60 Hz	Voltage: 0.05° typ., < 0.15° guar. Current: 0.1° typ., < 0.25° guar.[2]
Analog inputs	
Number	6
Input impedance	47 kΩ
Input voltage range (selectable)	±10 Vpeak (7.071 Vrms) ±7.071 Vpeak (5 Vrms)
Galvanic isolation input/output	Yes
Power supply	
Nominal input voltage[3]	100 – 240 VAC, 1-phase
Permissible input voltage	85 ... 264 VAC
Nominal frequency	50/60 Hz
Permissible frequency range	45 ... 65 Hz
Rated current	12 A at 115 V / 10 A at 230 V
Connection	Standard AC socket (IEC 60320)
Environmental conditions	
Operation temperature[4]	0 ... +50 °C (+32 ... +122 °F)
Storage temperature	-25 ... +70 °C (-13 ... +158 °F)
Humidity range	Relative humidity 5 ... 95 %, non-condensing
Vibration	IEC 60068-2-6 (20 m/s² at 10 ... 150 Hz)
Shock	IEC 60068-2-27 (15 g/11 ms half-sine)
Acoustics – noise emission Idle – full load	ISO 7779 47 – 55 dB(A)
Safety standards, electromagnetic compatibility	
EMC	The product adheres to the electromagnetic compatibility (EMC) Directive 2014/30/EU (CE conform).
International	IEC 61326-1; IEC 61000-4/6; IEC 61000-3-2/3
USA	FCC Subpart B of Part 15 Class A
Safety	The product adheres to the low voltage Directive 2014/35/EU (CE conform).
International / USA	IEC 61010-1 / UL 61010-1
Canada	CAN/CSA-C22.2 No 61010-1

Figure A.2 Technical data of CMS-356

B. Relay connections

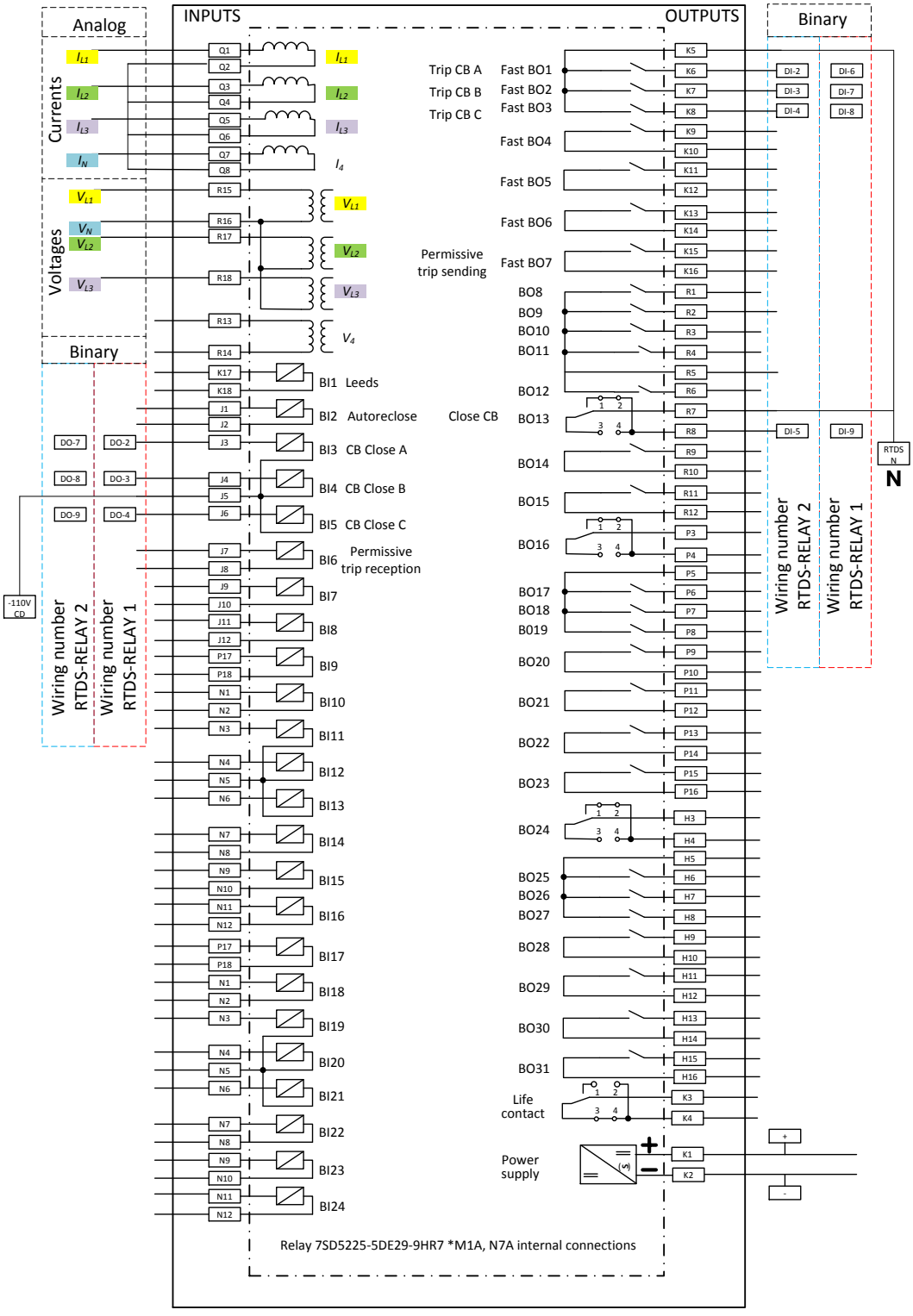

Figure B.1 Relay connections topology

C. Scripts

C.1 Script for relay testing in RSCAD

```
// definition of slider variables

float P_index[8],Res[4];

Res[0]=0.1;
Res[1]=1;
Res[2]=10;
Res[3]=300;

P_index[0]=50;
P_index[1]=70;
P_index[2]=75;
P_index[3]=77;
P_index[4]=80;
P_index[5]=82;
P_index[6]=85;
P_index[7]=90;

//definition of variables for folders and plots creation

int i,j,m;

string route,Q,W,E,R,T,Y,filename[6],filename_2,t[11],dist[8],resistance[4];


//filename is variable for 6 different plot names; filename_2 - for file type name;

filename[0]="\N10_N11_N12_lower_relay";
filename[1]="\I40_ABC_lower_relay";
filename[2]="\N34_N35_N36_upper_relay";
filename[3]="\I4_ABC_upper_relay";
filename[4]="\Trip_Reclosing_lower_relay";
filename[5]="\Trip_Reclosing_upper_relay";
filename_2=".mpb";

//t is variable for 11 faults names in one folder

t[0]="A_ground";
t[1]="B_ground";
t[2]="C_ground";
t[3]="AB_ground";
t[4]="BC_ground";
t[5]="AC_ground";
t[6]="ABC_ground";
t[7]="AB_interphase";
t[8]="BC_interphase";
t[9]="AC_interphase";
t[10]="ABC_interphase";

// route defines path to folder where you want to store data;
//change to 1, 2, 3, 4, 5, 6;

route="D:\2\";

// resistance is variable for 4 folders names in main folder e.g 3

resistance[0]="Resistance_0.1_Ohm";
resistance[1]="Resistance_1_Ohm";
resistance[2]="Resistance_10_Ohm";
resistance[3]="Resistance_300_Ohm";

// dist is variable defininig 8 folders names in each resistance folders;

dist[0]="\50_percent_of_line";
dist[1]="\70_percent_of_line";
dist[2]="\75_percent_of_line";
dist[3]="\77_percent_of_line";
dist[4]="\80_percent_of_line";
```

```
dist[5]="\82_percent_of_line";
dist[6]="\85_percent_of_line";
dist[7]="\90_percent_of_line";

//script for folders creation;

for (m=0;m<4;m=m+1){
 newFolder(route::resistance[m]);
    for (j=0;j<8;j=j+1){
    newFolder(route::resistance[m]::dist[j]);
   }// End j
}// End m

//script for RSCAD testing main body

m=1; //change to 0,1,2,3 in case of simulation continuation with different resistance
while (m<4){
j=0; //change to 0,1,2,3,4,5,6,7 in case of simulation continuation with different distance of fault location
    while (j<8){
            i=0;
       while (i<11){

                SetSwitch "Subsystem #1 : CTLs : Inputs : BRKA102" = 0;
                SetSwitch "Subsystem #1 : CTLs : Inputs : BRKB102" = 0;
                SetSwitch "Subsystem #1 : CTLs : Inputs : BRKC102" = 0;
                SetSwitch "Subsystem #1 : CTLs : Inputs : BRKA1002" = 0;
                SetSwitch "Subsystem #1 : CTLs : Inputs : BRKB1002" = 0;
                SetSwitch "Subsystem #1 : CTLs : Inputs : BRKC1002" = 0;
                SetSwitch "Subsystem #1 : CTLs : Inputs : N10toN11" = 0;
                SetSwitch "Subsystem #1 : CTLs : Inputs : N10toN12" = 0;
                SetSwitch "Subsystem #1 : CTLs : Inputs : BLOCKpv" = 0;

                SetSlider "DraftVariables : FaultResistance" = Res[m];
                SetSlider "DraftVariables : Dist5656" = P_index[j];     //initial state before start



                    if (i==0){
            SUSPEND 0.15;
                SetSwitch "Subsystem #1 : CTLs : Inputs : BRKA102" = 1;
                    }
                if(i==1){
                    SUSPEND 0.15;
                    SetSwitch "Subsystem #1 : CTLs : Inputs : N10toN11" = 1;
                    SetSwitch "Subsystem #1 : CTLs : Inputs : BRKB102" = 2;
                    }
                if(i==2){
                    SUSPEND 0.15;
                    SetSwitch "Subsystem #1 : CTLs : Inputs : N10toN12" = 1;
                    SetSwitch "Subsystem #1 : CTLs : Inputs : BRKC102" = 4;
                    }
                if(i==3){
                    SetSwitch "Subsystem #1 : CTLs : Inputs : BRKA102" = 1;
                SetSwitch "Subsystem #1 : CTLs : Inputs : BRKB102" = 2;
                    }
                if(i==4){
                    SetSwitch "Subsystem #1 : CTLs : Inputs : N10toN11" = 1;
                SetSwitch "Subsystem #1 : CTLs : Inputs : BRKB102" = 2;
                SetSwitch "Subsystem #1 : CTLs : Inputs : BRKC102" = 4;
                    }
                if(i==5){
                SetSwitch "Subsystem #1 : CTLs : Inputs : N10toN12" = 1;
                    SetSwitch "Subsystem #1 : CTLs : Inputs : BRKA102" = 1;
                SetSwitch "Subsystem #1 : CTLs : Inputs : BRKC102" = 4;
                    }
                if(i==6){
                    SetSwitch "Subsystem #1 : CTLs : Inputs : BRKA102" = 1;
                SetSwitch "Subsystem #1 : CTLs : Inputs : BRKB102" = 2;
                SetSwitch "Subsystem #1 : CTLs : Inputs : BRKC102" = 4;
                    }
                if (i==7){
                    SetSwitch "Subsystem #1 : CTLs : Inputs : BRKA1002" = 8;
                    }
                if(i==8){
```

```
                        SetSwitch "Subsystem #1 : CTLs : Inputs : N10toN11" = 1;
                                SetSwitch "Subsystem #1 : CTLs : Inputs : BRKB1002" = 16;
                                }
                        if(i==9){
                        SetSwitch "Subsystem #1 : CTLs : Inputs : N10toN12" = 1;
                                SetSwitch "Subsystem #1 : CTLs : Inputs : BRKC1002" = 32;
                                }
                        if(i==10){
                                SetSwitch "Subsystem #1 : CTLs : Inputs : BRKA1002" = 8;
                        SetSwitch "Subsystem #1 : CTLs : Inputs : BRKB1002" = 16;
                        SetSwitch "Subsystem #1 : CTLs : Inputs : BRKC1002" = 32;
                        }                                       //logic for 11 faults

                                        Start;

                SUSPEND 0.15;
                PushButton "Subsystem #1 : CTLs : Inputs : close4";
        SUSPEND 0.15;
        ReleaseButton "Subsystem #1 : CTLs : Inputs : close4";
        SUSPEND 0.15;
        PushButton "Subsystem #1 : CTLs : Inputs : close40";
        SUSPEND 0.15;
        ReleaseButton "Subsystem #1 : CTLs : Inputs : close40";   //closing the line with breakers
                SUSPEND 0.15;
                SetSwitch "Subsystem #1 : CTLs : Inputs : BLOCKpv" = 1; // ativate in case of PV connection or delete for generator
connection case
        SUSPEND 5;

                SUSPEND 0.15;
                PushButton "Subsystem #1 : CTLs : Inputs : PB1012";
                SUSPEND 0.15;
                ReleaseButton "Subsystem #1 : CTLs : Inputs : PB1012";
                SUSPEND 0.5;                                    //triger for fault creation


        Q=route::resistance[m]::dist[j]::filename[0]::t[i]::filename_2;
                W=route::resistance[m]::dist[j]::filename[1]::t[i]::filename_2;
                E=route::resistance[m]::dist[j]::filename[2]::t[i]::filename_2;
                R=route::resistance[m]::dist[j]::filename[3]::t[i]::filename_2;
                T=route::resistance[m]::dist[j]::filename[4]::t[i]::filename_2;
                Y=route::resistance[m]::dist[j]::filename[5]::t[i]::filename_2; //variables for plots creation

                SavePlot "N10_N11_N12_lower_relay",Q;
        SavePlot "I40_ABC_lower_relay",W;
        SavePlot "N34_N35_N36_upper_relay",E;
        SavePlot "I4_ABC_upper_relay",R;
        SavePlot "Trip_Reclosing_lower_relay",T;
        SavePlot "Trip_Reclosing_upper_relay",Y;                //saving of the plots

                Stop;

                        i=i+1;
        }// End i
                j=j+1;
    }// End j
m=m+1;
}// End m
```

C.2 Script for Matlab plotting

```
clear;
clc;

%name of the faults file

fault{1}='A_ground';
fault{2}='B_ground';
fault{3}='C_ground';
fault{4}='AB_ground';
fault{5}='BC_ground';
fault{6}='AC_ground';
```

```
fault{7}='ABC_ground';
fault{8}='AB_interphase';
fault{9}='BC_interphase';
fault{10}='AC_interphase';
fault{11}='ABC_interphase';

%variables for directories

distance='50'; %change to 50, 70, 75, 77, 80, 82, 85, 90;
Resistance='0.1'; %change to 0.1, 1, 10, 300;
tryy='1';%change to 1, 2, 3, 4, 5, 6;

for i=1:11

% 6 graphics directories

M = importdata(['D:\' tryy '\Resistance_' Resistance '_Ohm\' distance '_percent_of_line\I40_ABC_lower_relay' fault{i} '.out'], ' ', 1);
M1 = importdata(['D:\' tryy '\Resistance_' Resistance '_Ohm\' distance '_percent_of_line\I4_ABC_upper_relay' fault{i} '.out'], ' ', 1);
M2 = importdata(['D:\' tryy '\Resistance_' Resistance '_Ohm\' distance '_percent_of_line\N10_N11_N12_lower_relay' fault{i} '.out'], ' ', 1);
M3 = importdata(['D:\' tryy '\Resistance_' Resistance '_Ohm\' distance '_percent_of_line\N34_N35_N36_upper_relay' fault{i} '.out'], ' ', 1);
M4 = importdata(['D:\' tryy '\Resistance_' Resistance '_Ohm\' distance '_percent_of_line\Trip_Reclosing_lower_relay' fault{i} '.out'], ' ', 1);
M5 = importdata(['D:\' tryy '\Resistance_' Resistance '_Ohm\' distance '_percent_of_line\Trip_Reclosing_upper_relay' fault{i} '.out'], ' ', 1);

% figure description

h=figure('Name',fault{i},'NumberTitle','off');
%h=figure('Name',fault{i},'NumberTitle','off','visible','off');

% plot 1 description I40_ABC_lower_relay

A=M.data;
time=A(:,1);
phaseA=A(:,2);
phaseB=A(:,3);
phaseC=A(:,4);
subplot(3,2,1);
plot(time,phaseA,'k-',time,phaseB,'r--',time,phaseC,'b-.');
title('Current ABC Relay 1');
xlabel('Time,(s)');
ylabel('Current,(kA)');
legend('phase A','phase B','phase C');
grid on;

% plot 2 description Current I4 ABC upper relay

A1=M1.data;
time1=A1(:,1);
phaseA1=A1(:,2);
phaseB1=A1(:,3);
phaseC1=A1(:,4);
subplot(3,2,2);
plot(time1,phaseA1,'k-',time1,phaseB1,'r--',time1,phaseC1,'b-.');
title('Current ABC Relay 2');
xlabel('Time,(s)');
ylabel('Current,(kA)');
legend('phase A','phase B','phase C');
grid on;

% plot 3 description Voltage N10 N11 N12 lower relay

A2=M2.data;
time2=A2(:,1);
phaseA2=A2(:,2);
phaseB2=A2(:,3);
phaseC2=A2(:,4);
subplot(3,2,3);
plot(time2,phaseA2,'k-',time2,phaseB2,'r--',time2,phaseC2,'b-.');
title('Voltage N10 N11 N12 lower relay');
xlabel('Time in seconds');
ylabel('Voltage in kV');
legend('phase A','phase B','phase C');
grid on;

% plot 4 description Voltage N34 N35 N36 upper relay
```

```
A3=M3.data;
time3=A3(:,1);
phaseA3=A3(:,2);
phaseB3=A3(:,3);
phaseC3=A3(:,4);
subplot(3,2,4);
plot(time3,phaseA3,'k-',time3,phaseB3,'r--',time3,phaseC3,'b-.');
title('Voltage N34 N35 N36 upper relay');
xlabel('Time in seconds');
ylabel('Voltage in kV');
legend('phase A','phase B','phase C');
grid on;

% plot 5 description Trip and Reclosing lower relay

A4=M4.data;
time4=A4(:,1);
phaseA4=A4(:,2);
phaseB4=A4(:,3);
phaseC4=A4(:,4);
reclosing4=A4(:,5);
subplot(3,2,5);
plot(time4,phaseA4,'k-',time4,phaseB4,'r--',time4,phaseC4,'b-.',time4,reclosing4,'g-');
title('Trip and Reclosing Relay 1');
xlabel('Time,(s)');
ylabel('p.u.');
legend('phase A','phase B','phase C','reclosing');
grid on;

% plot 6 description Trip and Reclosing upper relay

A5=M5.data;
time5=A5(:,1);
phaseA5=A5(:,2);
phaseB5=A5(:,3);
phaseC5=A5(:,4);
reclosing5=A5(:,5);
subplot(3,2,6);
plot(time5,phaseA5,'k-',time5,phaseB5,'r--',time5,phaseC5,'b-.',time5,reclosing5,'g-');
title('Trip and Reclosing Relay 2');
xlabel('Time,(s)');
ylabel('p.u.');
legend('phase A','phase B','phase C','reclosing');
grid on;

hold on;
%saving if the figure and it's directory

savefig(['D:\' tryy '\Resistance_' Resistance '_Ohm\' distance '_percent_of_line\' fault{i}]);

% saveas(h,fault{i},'fig')
% saveas(h,fault{i},'jpg')
end;
```